ZAMM

ORIGINAL PAPER

Heatline visualization of natural convection heat transfer for nanofluids confined within parallelogrammic cavities in presence of discrete isoflux sources

Ahmed Hadi Hussain[1] | **Ali Meer Ali Al-Zamily**[2] | **Farooq Hassan Ali**[2] |
Salam Hadi Hussain[3]

[1] Department of Energy Engineering, College of Engineering-Al Musayab, University of Babylon, Babil, Iraq

[2] Department of Mechanical Engineering, College of Engineering, University of Babylon, Babil, Iraq

[3] Department of Automobile Engineering, College of Engineering-Al Musayab, University of Babylon, Babil, Iraq

Correspondence
Ahmed Hadi Hussain, Department of Energy Engineering, College of Engineering-Al Musayab, University of Babylon, Iraq.
Email: ahmedhadi99@yahoo.com

Natural convection in a parallelogrammic enclosure filled with different types of nanofluids (Al_2O_3, Ag and TiO_2) subjected to three discrete heated isoflux is examined numerically by using a heatlines visualization method. The position of three discrete isoflux are at left and right sidewalls remark by ($\lambda = 0.25$), while the third isoflux at a bottom wall remark by ($\zeta = 0.5$). The top wall with the remaining regions in the bottom wall is insulated, while the remaining regions in the side walls are maintained at low temperatures. Finite element method based on a Chorin's algorithm used to solve the governing equation continuity, momentum and energy. Numerical calculations were achieved for a wide range of Rayleigh numbers ($10^4 \leq Ra \leq 10^7$), skew angle ($-30^o \leq \gamma \leq +30^o$), and volume fraction of nanoparticles ($0 \leq \Phi \leq 0.2$). The result is explained in term of stream functions, isotherms, heatfunctions, local and average Nusselt numbers. It is found that the heat transfer performance considerably improve with the supplement water of various species of nanofluid and changing skew angle. Furthermore, nine correlations are established to approximate the average Nusselt number.

KEYWORDS
heatflux, heatfunction, nanofluids, natural convection, parallelogram enclosure

1 | INTRODUCTION

Natural convection can see it in many engineering applications [1–9] such as cooling electronic paraphernalia, solar energy accumulators and distillation, nuclear energy, heating and cooling buildings, oven electronics, system lubrication, units of heat exchangers, methods of solidification and melting, etc. Natural convection heat transfer phenomenon in different closed shapes such as square, rectangular, cylindrical, triangular or parallelogram is substantial engineering attention. Numerical study deals with natural convection in regular enclosures containing air, water and nanofluids with numerous boundary conditions are obtained in many recent papers [10–13]. Earlier experimental study for free convection heat transfer in parallogrammic enclosure for different tilt angles, Prandtl number and Rayleigh number have been established by Seki et al. [14]. Heat transfer by natural convection in parallelogram cavity with air as a working fluid have studied by [15–22].While, other studies involve natural convection in a porous media [23–25]. Latest natural convection in rhombic enclosures with isothermal hot side or bottom wall has been studied by Anandalakshmi and Basak [26–27]. Bäiri et al. [28–29] investigated experimental and numerical transient 2D natural convection in parallelogrammic enclosures which practiced to the on-board electronics and thermoregulation of avionics. Bäiri et al. [30] worked a literature review on natural convection in enclosures for engineering applications. In this study, the natural convection in parallelogram enclosure is given in detail. Hussain et al. [31] studied the natural convection heat transfer in parallelogram geometry with heat generation and non-uniformly heated left sidewall and right cooled side wall while the top and bottom walls are adiabatic. Jagadeesha et al. [32,33] conducted a numerical study for a double diffusive natural convection in parallelogrammic enclosure filled with a porous medium. In the first study the heated side walls and adiabatic top and bottom walls. For second study the influence of the magnetic strength was considered along the horizontal direction (x-axis). Das et al. [34] performed a literature survey for natural convection within enclosures of various (non-square) shapes. This work assists the researchers in selecting realistic cavity and seemly experimental and numerical case study.

In the past few years ago, the latest literature review papers deal with the enhancing heat transfer by nanofluids have been great attention. Basak and Chamkha [35] have been investigated based on visualization of heat flow via heatfunctions the effect of nanofluid natural convection in a square enclosure in presence of hot and cold side walls (case 1) or uniform or non-uniform heating of bottom wall with cold side walls (case 2). Oztop et al. [36] analyzed heat and fluid flow in an inclined non-uniformly heated square enclosure filled with CuO nanofluid. The parameters studied are nanoparticle volume fraction and angle of inclination. Morad et al. [37] studied two objects in this experimental work, the first object to investigate the existence or not nanoparticle addition has a positive or negative effect of natural convection heat transfer. The second objective to studied effect of angle of inclination and aspect ratio. Hussain and Hussein [38] studied the laminar natural heat transfer and fluid flow inside the parallelogrammic enclosure filled with water-copper nanofluids. The heated wall boundary condition is assumed in this study. Ghalambaz et al. [39] examined the influence of the existence of nanofluid and porous medium in a parallelogrammic enclosure with the heated side walls. Alsabery et al. [40] extended heatline analysis by natural convection in a trapezoidal enclosure divided in two parts, one filled with porous nanofluid and second part filled with nano-Newtonian fluid. Selimefendigil et al. [41] examined the natural convection and entropy generation in entrapped trapezoidal enclosures filled with nanofluids under the influence of magnetic field. Alsabery et al. [42] solved the problem of conjugate natural convection a square cavity for four different nanofluid particles with sinusoidal temperature variations on both horizontal walls. Wang and Dai [43] have been investigated the natural convection heat transfer and convective flow of nanofluids in inclined enclosures from a heated thin plate located in the middle of an inclined enclosure filled water-based different kind of nanofluids. Mehryan et al. [44] examined the natural convection heat transfer of the Al_2-O_3-Cu water hybrid nanofluid in a square enclosure filled with a porous medium. The results show that the reduction percentage of the heat transfer rate of a hybrid nanofluid is much more than that for a single regular nanofluid. For researchers which interested in hybrid nanofluids, Syam Sunder et al. [45] makes a review with hybrid nanoparticles. This review examined the thermo-physical properties, heat and friction coefficient. Natural convection in a closed enclosure with district heating have studied by numbers of researchers with different numbers and positions or heating elements [46–48].

The natural convection in a closed enclosure due to discrete heat source is a common engineering case such as cooling electronics, heating or cooling buildings, etc. The ancient papers deals with natural convection in a closed enclosure due to discrete isoflux are [49–55]. Narasimham [56] reported on natural convection from discrete heat source in enclosures and directions for further researchers are mentioned. Baïri et al. [58] examined the thermal behavior of air born electronic equipment submitted to natural convection in closed parallelogrammic air-filled. Three discrete active bands generating a constant heat in vertically one side of the enclosure is designed. Sankar et al. [59] investigated numerical study of double diffusive convection in a vertical annulus filled with fluid-saturated porous medium. Takabi and Salehi

F I G U R E 1 Description of the present study
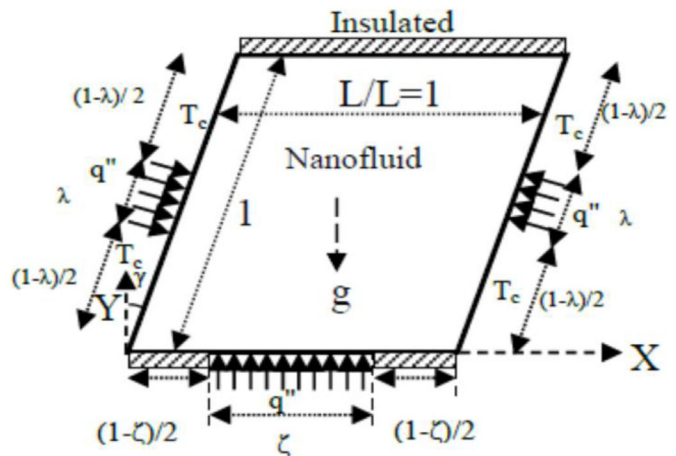
[60] established numerical study of natural convection in a sinusoidal corrugated enclosure in presence of discrete heat source, filled with hybrid nanofluid. The results show that the employing hybrid nanofluid improves the heat transfer rate compared to nanofluid. Elsherbiny [61] studied the natural convection in differentially heated rectangular enclosures filled with air. The parameters studied were the tilt angle, aspect ratio, position ratio and size ratio with a range of the Rayleigh number between 10^3 and 10^6. A correlation of average Nusselt number was attained. Cho et al. [62] investigated numerically the natural convection and entropy generation in a U-shape cavity filled with Al_2O_3-water with nanofluid. Simulation deals with the effect of the solid volume fraction, Rayleigh number and the geometric shape of the heat transfer performance. Das and Basak [63] conducted entropy generation within square and triangular enclosures subjected to two discrete heating from the side wall. Hussein and Hussain [64] worked numerical study for natural convection visualization of heat lines in the tilting wavy enclosure of various configurations occupied with nanofluids. Nithyadevi et al. [65] studied the effect of Prandtl number on the natural convection inside a rectangular enclosure with more than one discrete heater in the left sidewall in the presence of an internal heat generation. It is found that the Prandtl number and the number of discrete heaters have a significant role on the heat transfer and fluid flow inside the enclosure. Oztop and Abu-Nada [66] conducted a numerical study of natural convection inside the rectangular enclosure, partially heated from the left horizontal wall and filled with various types of metallic nanofluid (Cu, Al_2O_3, TiO_2). Results show that utilizing nanofluid augmented heat transfer and its more effected on low aspect ratio compared to high aspect ratio. Bondareva et al. [67] examined numerically free convection of Copper-water in an open triangular cavity with entropy generation. The cavity heated partially by a hot element in the bottom wall. Results show that increase Rayleigh number, additive Cu-nanoparticles enhanced heat transfer, displacement heat element to the left enhanced heat transfer rate. Shermet et al. [68] studied free convection heat transfer and entropy generation inside a cavity having a sinusoidal right wall using finite difference approach. Copper-water is used as a working fluid with the single phase model. Selimefendigil and Oztop [69] investigated mixed convection in three-dimensional cubic geometry filled with nanofluid. Two adiabatic circular cylinders placed at the center of the cavity. Three different types of nanofluid are used (copper, aluminum oxide, titanium oxide). Higher heat transfer obtained at higher Ryleigh number with Copper nanofluid.

From the above literature review and from our knowledge in natural convection in a closed enclosure, no study of the researchers transactions is performed up to date with employed heatlines visualization by natural convection in a parallelogrammic enclosure filled with three types of nanofluids in the presence of three isoflux heat sources, two in sidewalls and third in the bottom wall. Also, no work gives a comparison in streamlines, isotherms, heatlines, local and average numbers between three different kinds of nanofluid. The major originality of this paper is dealing with streamfunction, isotherm and heat function in non-regular shape (parallelogrammic enclosure) with different types of nanofluids in the presence of more than one or two side walls isoflux boundary conditions. The additional parameters studied are Rayleigh number ($10^4 \leq Ra \leq 10^7$), skew angle ($-30^o \leq \gamma \leq +30^o$) and solid volume fraction of nanoparticle ($0 \leq \Phi \leq 0.2$).

2 | PROBLEM DESCRIPTION

The considered cavity is exemplified in Figure 1. It is a parallelogrammic cavity which has width and height equal to unity. The vertical walls (left and right) inclined by an angle vary from -30° to $+30^o$. The top wall and two partitions on the

bottom wall are adiabatic. Three discrete isoflux heating element are inserted in left, right walls with same dimensions equal to ($\lambda = 0.25$) and at the bottom wall equal to ($\zeta = 0.5$), the rest of the left and right walls are kept at cold temperatures.

3 | MATHEMATICAL EXPRESSION AND SIMULATION

3.1 | Velocity and temperature fields

The statements governing equations for time-independent (steady-state), two-dimensional, free convection heat transfer and fluid flow in the parallelogram cavity using continuity, momentum and energy described with next dimensionless variables [56]:

$$X = \frac{x}{L}, \quad Y = \frac{y}{L}, \quad U = \frac{uL}{\alpha_f}, \quad V = \frac{vL}{\alpha_f}, \quad P = \frac{pL^2}{\rho_{nf}\alpha_f^2}, \quad \theta = \frac{T - T_c}{\Delta T}, \quad \Delta T = \frac{qL}{k_f}, \quad Ra = \frac{g\beta_f L^3 \Delta T}{\nu_f \alpha_f},$$

$$Pr = \frac{\nu_f}{\alpha_f}, \quad \frac{\partial U}{\partial X} + \frac{\partial V}{\partial Y} = 0 \tag{1}$$

$$U\frac{\partial U}{\partial X} + V\frac{\partial U}{\partial Y} = -\frac{\partial P}{\partial X} + \frac{\mu_{nf}}{\rho_{nf}\alpha_f}\left(\frac{\partial^2 U}{\partial X^2} + \frac{\partial^2 U}{\partial Y^2}\right) \tag{2}$$

$$U\frac{\partial V}{\partial X} + V\frac{\partial V}{\partial Y} = -\frac{\partial P}{\partial Y} + \frac{\mu_{nf}}{\rho_{nf}\alpha_f}\left(\frac{\partial^2 V}{\partial X^2} + \frac{\partial^2 V}{\partial Y^2}\right) + \frac{(\rho\beta)_{nf}}{\rho_{nf}\beta_f}Ra\,Pr \tag{3}$$

$$U\frac{\partial \theta}{\partial X} + V\frac{\partial \theta}{\partial Y} = \frac{\alpha_{nf}}{\alpha_f}\left(\frac{\partial^2 \theta}{\partial X^2} + \frac{\partial^2 \theta}{\partial Y^2}\right) \tag{4}$$

Here, ρ_{nf} is the density of the nanofluid expressed as:

$$\rho_{nf} = (1 - \Phi)\ \rho_f + \Phi\,\rho_p \tag{5}$$

Allowing to Brinkman's expression [70], the dynamic viscosity of the nanofluid is formed as:

$$\mu_{nf} = \frac{\mu_f}{(1 - \Phi)^{2.5}} \tag{6}$$

The coefficient of thermal expansion of the nanofluid can be found by:

$$(\rho\beta)_{nf} = (1 - \Phi)\ (\rho\beta)_f + \Phi(\rho\beta)_p \tag{7}$$

Nanofluid thermal diffusivity is expressed by:

$$\alpha_{nf} = \frac{k_{nf}}{(\rho C_p)_{nf}} \tag{8}$$

where k_{nf} is the thermal conductivity of the nanofluid, which for spherical shape nanometallic is expressed by Maxwell [71]:

$$k_{nf} = k_f\frac{(k_p + 2k_f) - 2\Phi(k_f - k_p)}{(k_p + 2k_f) + \Phi(k_f - k_p)} \tag{9}$$

The capacity of heat of the nanofluid is defined as:

$$(\rho C_p)_{nf} = (1 - \Phi)\ (\rho C_p)_f + \Phi(\rho C_p)_p \tag{10}$$

TABLE 1 Thermo-physical properties of water (base fluid) and nanometallic

Properties	Pure water	Silver (Ag)	Alumina (Al$_2$O$_3$)	Titanium oxide (TiO$_2$)
Cp (J/kg.K)	4179	235	765	686.2
K (W/m.K)	0.613	429	40	8.9538
ρ (kg/m^3)	997.1	10,500	3970	4250
β(1/K) $\times 10^5$	21	1.89	0.85	0.9

In the previous functions, subscripts (f) and (p) are related to base fluid (water) and dispersed nanometallic, respectively. The thermo-physical properties of the base fluid and the considered nanoparticles in this work are specified in Table 1 as stated in [56].

The local Nusselt number on the heat sources can be defined as follows:

$$Nu = \frac{hL}{k_f} \tag{11}$$

where, h is the heat transfer coefficient:

$$h = \frac{q''}{T_s - T_c} \tag{12}$$

Rearranging the local Nusselt number by using the temperature dimensionless, yields:

$$Nu = \frac{1}{\theta|_{\text{heat source wall}}} \tag{13}$$

Integrated local Nusselt number along the heat source will produce average Nusselt number $(\overline{Nu})$ as.

$$\overline{Nu} = \frac{\int_{\text{along}}^{\text{heat source}} Nu \, dn}{\int_{\text{along}}^{\text{heat source}} dn} \tag{14}$$

At bottom wall:

$$\overline{Nu}_b = \frac{1}{\zeta} \int_{0.5(1-\zeta)}^{0.5(1+\zeta)} Nu \, dn \tag{15}$$

At left or right side wall:

$$\overline{Nu}_{\text{L or R}} = \frac{1}{\lambda} \int_{0.5(1-\lambda)}^{0.5(1+\lambda)} Nu \, dn \tag{16}$$

3.2 | Stream function and heat function

The fluid motion is displayed using the stream function (ψ) obtained from the velocity components U and V. The relationships between stream function, ψ [72] and velocity components for two-dimensional flows are:

$$U = \frac{\partial \psi}{\partial Y}, \quad V = -\frac{\partial \psi}{\partial X} \tag{17a}$$

$$\frac{\partial^2 \psi}{\partial X^2} + \frac{\partial^2 \psi}{\partial Y^2} = \frac{\partial U}{\partial Y} - \frac{\partial V}{\partial X} \tag{17b}$$

The no-slip condition is valid at all boundaries as there is no cross flow, hence $\psi = 0$ is used as residual equations at the nodes for the boundaries.

The heat flow within the enclosure is displayed using the heatfunction (Π) obtained from conductive (diffusive) heat fluxes $(-\frac{\partial\theta}{\partial X}, -\frac{\partial\theta}{\partial Y})$ as well as convective heat fluxes ($U\theta$, $V\theta$). The heatfunction satisfies the steady energy balance equation (Equation (4)) [68] such that:

$$\frac{\partial\Pi}{\partial Y} = U\theta - \frac{\alpha_{nf}}{\alpha_f}\frac{\partial\theta}{\partial X}, \quad -\frac{\partial\Pi}{\partial X} = V\theta - \frac{\alpha_{nf}}{\alpha_f}\frac{\partial\theta}{\partial Y} \tag{18}$$

Those yields a single equation,

$$\frac{\partial^2\Pi}{\partial X^2} + \frac{\partial^2\Pi}{\partial Y^2} = \frac{\partial}{\partial Y}(U\theta) - \frac{\partial}{\partial X}(V\theta) \tag{19}$$

Heatfunction boundary conditions are calculated from the Equation (18).

3.3 | Boundary conditions

The boundary conditions that combined with the governing Equations (1, 2, 3, 4, 9 and 11) for the present study are arranged, as follows:

(a) For left partition bottom adiabatic wall:

$$\text{For } Y = 0 \text{ and } 0 \leq X \leq 0.5(1-\zeta), \ U(X,0) = V(X,0) = 0, \ \frac{\partial\theta}{\partial Y} = 0, \ \psi = 0, \ \Pi = 0 \tag{20a}$$

(b) For discrete isoflux at bottom wall:

$$\text{For } Y = 0 \text{ and } 0.5(1-\zeta) \leq X \leq 0.5(1+\zeta), \ U(X,0) = V(X,0) = 0, \ \frac{\partial\theta}{\partial Y} = -\frac{k_f}{k_{nf}}, \ \psi = 0, \ -\frac{\partial\Pi}{\partial X} = \frac{k_f}{k_{nf}}\frac{\alpha_{nf}}{\alpha_f} \tag{20b}$$

(c) For right partition bottom adiabatic wall:

$$\text{For } Y = 0 \text{ and } 0.5(1+\zeta) \leq X \leq 1, \ U(X,0) = V(X,0) = 0, \ \frac{\partial\theta}{\partial Y} = 0, \ \psi = 0, \ \Pi = 0 \tag{20c}$$

(d) For lower partition left cold wall:

$$\text{For } X = 0 \text{ and } 0 \leq Y \leq 0.5(1-\lambda), \ U(0,Y) = V(0,Y) = 0, \ \theta = 0, \ \psi = 0, \ n.\nabla\Pi = 0 \tag{20d}$$

(e) For discrete isoflux at left wall:

$$\text{For } X = 0 \text{ and } 0.5(1-\lambda) \leq Y \leq 0.5(1+\lambda), \ U(0,Y) = V(0,Y) = 0, \ \frac{\partial\theta}{\partial n} = -\frac{k_f}{k_{nf}}, \psi = 0, n.\nabla\Pi = \frac{k_f}{k_{nf}}\frac{\alpha_{nf}}{\alpha_f} \tag{20e}$$

(f) For upper partition left cold wall:

$$\text{For } X = 0 \text{ and } 0.5(1-\lambda) \leq Y \leq 1, \ U(0,Y) = V(0,Y) = 0, \ \theta = 0, \ \psi = 0, \ n.\nabla\Pi = 0 \tag{20f}$$

(g) For lower partition right cold wall:

$$\text{For } X = 1 \text{ and } 0 \leq Y \leq 0.5(1-\lambda), \ U(1,Y) = V(1,Y) = 0, \ \theta = 0, \ \psi = 0, \ n.\nabla\Pi = 0 \tag{20g}$$

TABLE 2 The nanofluid (Cu-water) ($\Phi = 0.1$) ($\zeta = 0.4$), at base heat flux and insulated walls, others walls (slope and upper) at cold temperature

Ra	$\overline{Nu_b}$ [5]	Present	θ_{max} [5]	Present	ψ_{max} [5]	Present
10^3	5.45	5.56	0.205	0.21	0.023	0.022
10^4	5.47	5.57	0.205	0.202	0.251	0.248
10^5	7.12	7.19	0.172	0.171	2.988	2.96
10^6	13.8	13.42	0.107	0.107	11.593	11.5

(h) For discrete isoflux at right wall:

For $X = 1$ and $0.5(1-\lambda) \leq Y \leq 0.5(1+\lambda)$, $U(1,Y) = V(1,Y) = 0$, $\dfrac{\partial\theta}{\partial n} = -\dfrac{k_f}{k_{nf}}$, $\psi = 0$, $n.\nabla\Pi = \dfrac{k_f}{k_{nf}}\dfrac{\alpha_{nf}}{\alpha_f}$ (20h)

(i) For upper partition right cold wall:

For $X = 1$ and $0.5(1-\lambda) \leq Y \leq 1$, $U(1,Y) = V(1,Y) = 0$, $\theta = 0$, $\psi = 0$, $n.\nabla\Pi = 0$ (20i)

(j) For top adiabatic wall:

For $Y = 1$ and $0 \leq X \leq 1$, $U(X,1) = V(X,1) = 0$, $\dfrac{\partial\theta}{\partial Y} = 0$, $\psi = 0$, $\Pi = \displaystyle\int_0^1 \dfrac{\alpha_{nf}}{\alpha_f}\dfrac{\partial\theta}{\partial Y} \, dX$ (20j)

4 | NUMERICAL METHOD AND VALIDATION

The Navier-Stokes, energy, stream function and heat function equations are discredited using finite element method based on the variation formulation [73]. A development of Chorin's algorithms, specified by Rannacher is utilized in the current study to calculate the last time independent (steady state), velocity, temperature and pressure. This algorithm was recognized as the projection formula, normally, this algorithm involve two steps. In the first step, an intermediate velocity that does not fulfill the incompressibility restriction is calculated at each step. In the next step, the modification factor for pressure and velocity is calculated to obtain the subsequent update of velocity and pressure.

The current numerical approach is tested for accuracy with the published numerical paper of Aminossadati and Ghasemi [56] for natural convection cooling of a heat source embedded in the bottom wall of an enclosure filled with nanofluid. These results for the case (nanofluid: Cu- water, $\Phi = 0.1$, $\zeta = 0.4$) at base heat flux and insulated walls, others walls (inclined and upper) at cold temperature. The results for an average Nusselt number, maximum temperature and streamlines showed relative very low differences (see Table 2).

To check the grid-independence solutions, a series of trial calculation for the case: nanofluid (Ag-water) ($\Phi = 0.1$) ($\zeta = 0.5$) ($\lambda = 0.25$) ($\gamma = 0°$) ($Ra = 10^5$) was conducted for different grid distributions, that is, (10×10), (20×20), 30×30, (40×40), (50×50), (60×60), (70×70), (80×80), (90×90) and (100×100) (see Table 3). It was observed that the difference between the results of the grid (80×80) and that of the grid (100×100) is less than 0.01%. In order to optimize appropriate grid refinement with computational efficiency, the grid size (80×80) is chosen for all computations in the present work.

5 | RESULTS AND DISCUSSION

The results are performed for different values of the Rayleigh number ($10^4 \leq Ra \leq 10^7$), inclination sidewall angle ($-30° \leq \gamma \leq +30°$ step $15°$), nanofluid type (Silver (Ag) –Water, Alumina (Al$_2$O$_3$) –water and titanium oxide (TiO$_2$) –Water) and solid volume fraction of nanoparticles ($0 \leq \Phi \leq 0.2$ step 0.05). The working fluid water with (Pr = 6.2). The heat source, length ($\zeta = 0.5$, $\lambda = 0.25$) are considered. In all figures, the nanofluid represented by solid lines (———) and the pure water by dashed lines (- - - - -). The range of Rayleigh number considered in the present work covers the laminar convection heat transfer regime inside parallelogrammic cavity [15-25, 28–33, 38-39]. The present work has focused on studying the impact

TABLE 3 The nanofluid (Ag-water) at ($\Phi = 0.1, \varepsilon = 0.5, \lambda = 0.25, \gamma = 0°$ and $Ra = 10^5$)

Grid	$|\psi_{max}|$	θ_{max}	$|\Pi_{max}|$	$\overline{Nu_b}$
10×10	2.3373	0.16004	0.15371	7.7829
20×20	2.3197	0.15990	0.15387	7.7948
30×30	2.3207	0.16012	0.15463	7.7786
40×40	2.3107	0.16027	0.15437	7.7673
50×50	2.3055	0.16030	0.15404	7.7634
60×60	2.2967	0.16030	0.15358	7.7599
70×70	2.2921	0.16028	0.15324	7.7582
80×80	*2.2880*	*0.16026*	*0.15300*	*7.7558*
90×90	2.2879	0.16026	0.15298	7.7558
100×100	2.2878	0.16025	0.15297	7.7557
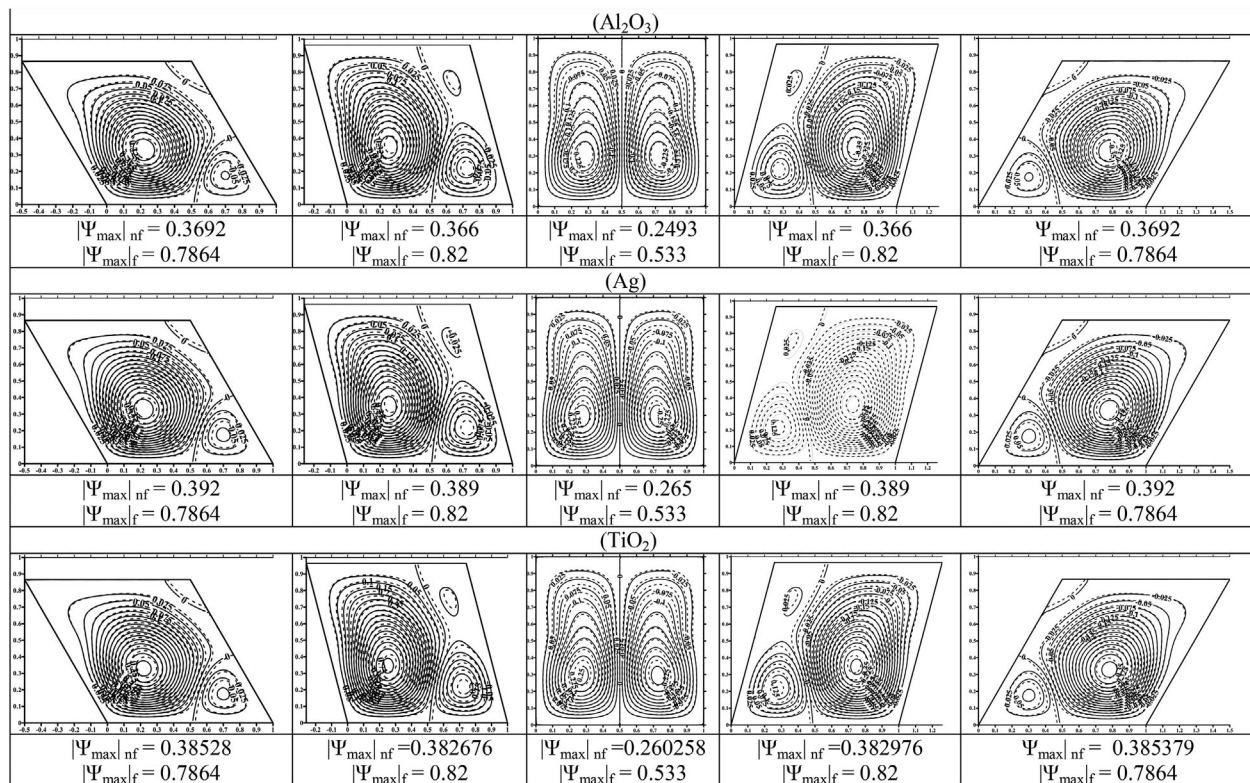
FIGURE 2 Streamfunction for different value of ($\gamma = -30°, -15°, 0°, 15°, 30°$) for nanofluid ($Al_2O_3$, Ag and TiO_2) at $\Phi = 0.1$ and $Ra = 10^4, \zeta = 0.5, \lambda = 0.25$, ——— nanofluid, _ _ _ _ pure water

of Rayleigh number, types of nanofluid, nanofluid volume fraction, inclination angle on the streamfunctuion, isotherms, heatfunction, nanofluid stability, in addition to local and average Nusselt number and heat transfer correlations for various parameters mentioned above was illustrated in Figures 2–15 and Tables 4-9.

5.1 | Effect of enclosure skew angle and Rayleigh number on flow field

Figure 2 represents the stream function in the parallelogrammic enclosure for different skew angles, starts from -30°, $-15^o, 0^o, 15^o, 30^o$ and three types of nanofluid Al_2O_3, Ag and TiO_3 based water at volume fraction ($\Phi = 0.1$) and Rayleigh number ($Ra = 10^4$). The maximum intensity of stream function signified by (Ψ_{max}). Due to gravitational force, the flow start to move from heat source regions in the bottom and sidewalls and flow towards a top insulating top wall. The coldest

(Al_2O_3)

$|\Psi_{max}|_{nf} = 12.3252$ $|\Psi_{max}|_{f} = 12.7037$	$|\Psi_{max}|_{nf} = 13.7754$ $|\Psi_{max}|_{f} = 14.7926$	$|\Psi_{max}|_{nf} = 9.21977$ $|\Psi_{max}|_{f} = 11.6169$	$|\Psi_{max}|_{nf} = 13.781$ $|\Psi_{max}|_{f} = 14.7931$	$|\Psi_{max}|_{nf} = 12.3257$ $|\Psi_{max}|_{f} = 12.8516$

(Ag)

$|\Psi_{max}|_{nf} = 13.1885$ $|\Psi_{max}|_{f} = 12.7037$	$|\Psi_{max}|_{nf} = 15.0423$ $|\Psi_{max}|_{f} = 14.7926$	$|\Psi_{max}|_{nf} = 9.75333$ $|\Psi_{max}|_{f} = 11.6169$	$|\Psi_{max}|_{nf} = 15.0458$ $|\Psi_{max}|_{f} = 14.7931$	$|\Psi_{max}|_{nf} = 13.1894$ $|\Psi_{max}|_{f} = 12.8516$

(TiO_2)

$|\Psi_{max}|_{nf} = 12.1495$ $|\Psi_{max}|_{f} = 12.7037$	$|\Psi_{max}|_{nf} = 13.6558$ $|\Psi_{max}|_{f} = 14.7926$	$|\Psi_{max}|_{nf} = 9.25154$ $|\Psi_{max}|_{f} = 11.6169$	$|\Psi_{max}|_{nf} = 13.6779$ $|\Psi_{max}|_{f} = 14.7931$	$|\Psi_{max}|_{nf} = 12.1764$ $|\Psi_{max}|_{f} = 12.8516$

FIGURE 3 Streamfunction for different value of ($\gamma = -30°, -15°, 0°, 15°, 30°$) for nanofluid ($Al_2O_3$, Ag and TiO_2) at $\Phi = 0.15$ and Ra = 10^6 $\zeta = 0.5$, $\lambda = 0.25$, —— nanofluid, _ _ _ _ pure water

(Al_2O_3)

$|\Psi_{max}|_{nf} = 25.571$ $|\Psi_{max}|_{f} = 23.601$	$|\Psi_{max}|_{nf} = 30.114$ $|\Psi_{max}|_{f} = 25.593$	$|\Psi_{max}|_{nf} = 25.415$ $|\Psi_{max}|_{f} = 20.054$	$|\Psi_{max}|_{nf} = 30.109$ $|\Psi_{max}|_{f} = 25.489$	$|\Psi_{max}|_{nf} = 25.566$ $|\Psi_{max}|_{f} = 23.553$

(Ag)

$|\Psi_{max}|_{nf} = 27.956$ $|\Psi_{max}|_{f} = 23.601$	$|\Psi_{max}|_{nf} = 34.135$ $|\Psi_{max}|_{f} = 25.593$	$|\Psi_{max}|_{nf} = 29.198$ $|\Psi_{max}|_{f} = 20.054$	$|\Psi_{max}|_{nf} = 34.112$ $|\Psi_{max}|_{f} = 25.489$	$|\Psi_{max}|_{nf} = 27.942$ $|\Psi_{max}|_{f} = 23.553$

(TiO_2)

$|\Psi_{max}|_{nf} = 24.956$ $|\Psi_{max}|_{f} = 23.601$	$|\Psi_{max}|_{nf} = 29.296$ $|\Psi_{max}|_{f} = 25.593$	$|\Psi_{max}|_{nf} = 25.174$ $|\Psi_{max}|_{f} = 20.054$	$|\Psi_{max}|_{nf} = 29.303$ $|\Psi_{max}|_{f} = 25.489$	$|\Psi_{max}|_{nf} = 24.961$ $|\Psi_{max}|_{f} = 23.553$

FIGURE 4 Streamfunction for different value of ($\gamma = -30°, -15°, 0°, 15°, 30°$) for nanofluid ($Al_2O_3$, Ag and TiO_2) at $\Phi = 0.2$ and Ra = 10^7 $\zeta = 0.5$, $\lambda = 0.25$, —— nanofluid, _ _ _ _ pure water
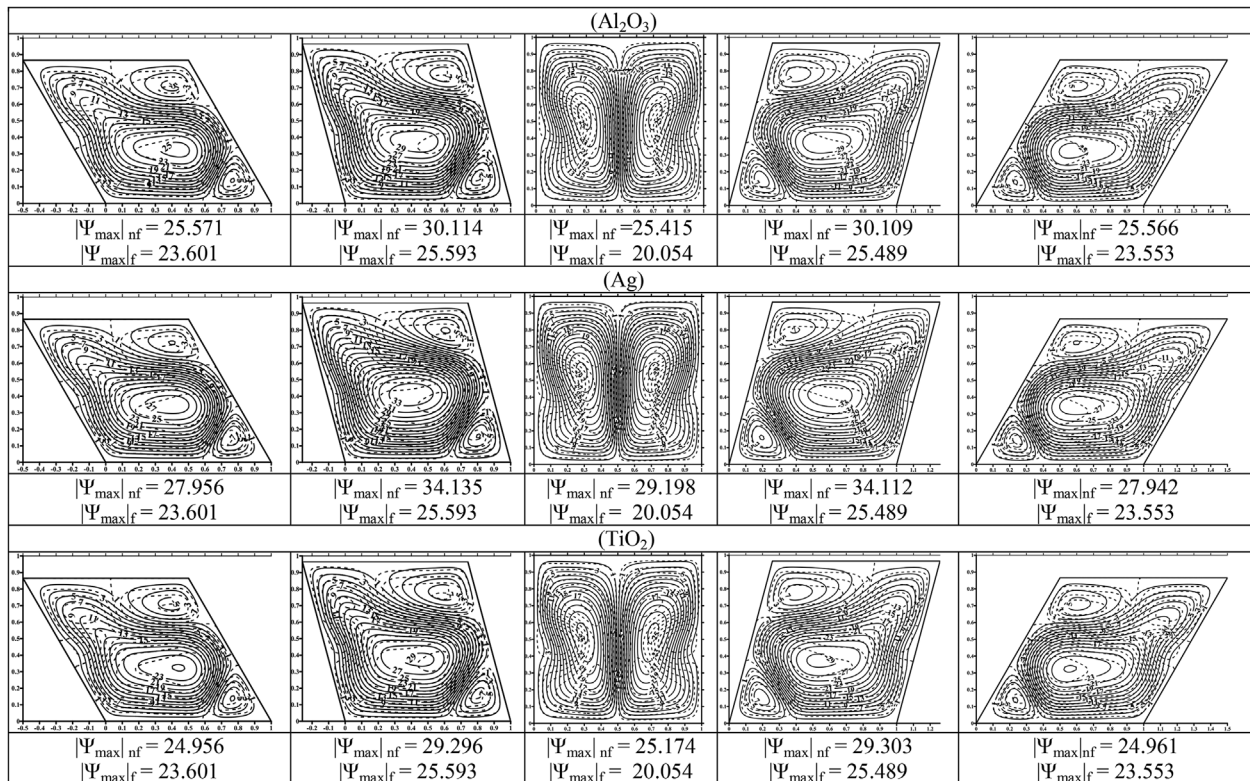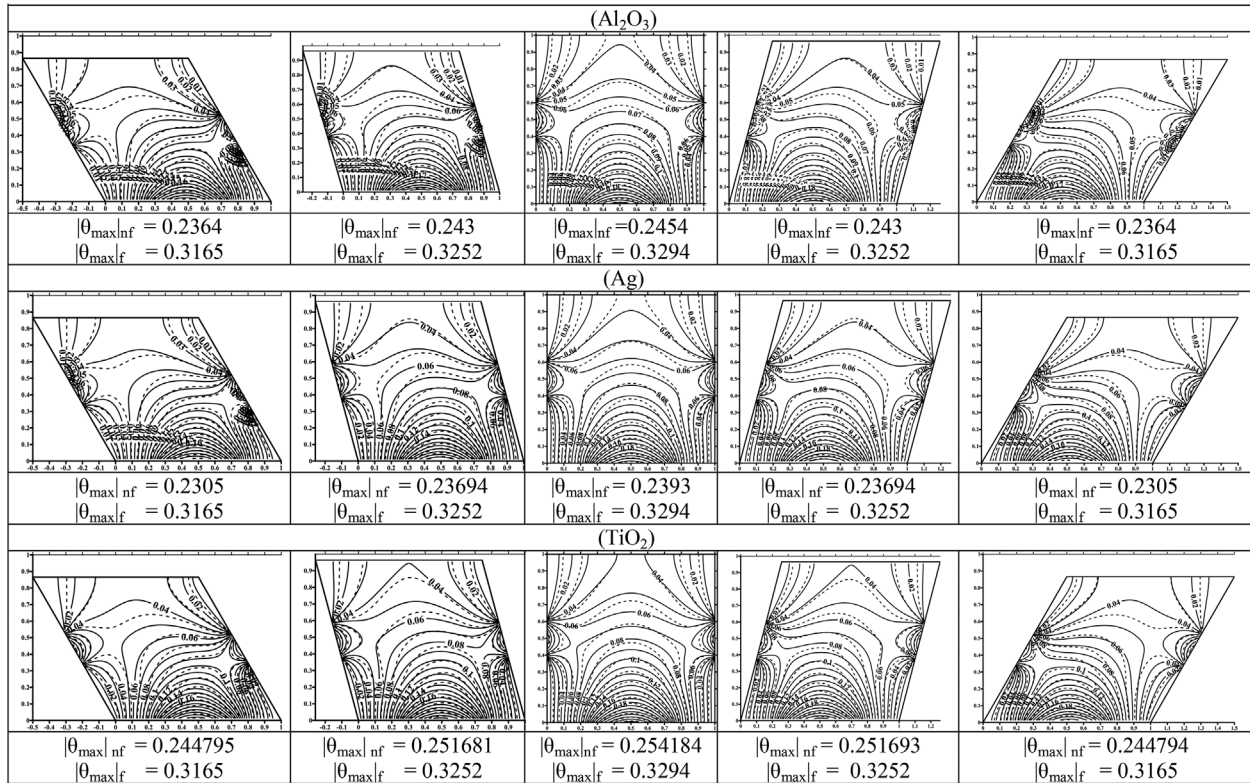
(Al₂O₃)				
$|\theta_{max}|_{nf} = 0.2364$ $|\theta_{max}|_{f} = 0.3165$	$|\theta_{max}|_{nf} = 0.243$ $|\theta_{max}|_{f} = 0.3252$	$|\theta_{max}|_{nf} = 0.2454$ $|\theta_{max}|_{f} = 0.3294$	$|\theta_{max}|_{nf} = 0.243$ $|\theta_{max}|_{f} = 0.3252$	$|\theta_{max}|_{nf} = 0.2364$ $|\theta_{max}|_{f} = 0.3165$
(Ag)				
$|\theta_{max}|_{nf} = 0.2305$ $|\theta_{max}|_{f} = 0.3165$	$|\theta_{max}|_{nf} = 0.23694$ $|\theta_{max}|_{f} = 0.3252$	$|\theta_{max}|_{nf} = 0.2393$ $|\theta_{max}|_{f} = 0.3294$	$|\theta_{max}|_{nf} = 0.23694$ $|\theta_{max}|_{f} = 0.3252$	$|\theta_{max}|_{nf} = 0.2305$ $|\theta_{max}|_{f} = 0.3165$
(TiO₂)				
$|\theta_{max}|_{nf} = 0.244795$ $|\theta_{max}|_{f} = 0.3165$	$|\theta_{max}|_{nf} = 0.251681$ $|\theta_{max}|_{f} = 0.3252$	$|\theta_{max}|_{nf} = 0.254184$ $|\theta_{max}|_{f} = 0.3294$	$|\theta_{max}|_{nf} = 0.251693$ $|\theta_{max}|_{f} = 0.3252$	$|\theta_{max}|_{nf} = 0.244794$ $|\theta_{max}|_{f} = 0.3165$

FIGURE 5 Isotherms for different value of ($\gamma = -30°, -15°, 0°, 15°, 30°$) for nanofluid (Al₂O₃, Ag and TiO₂) at $\Phi = 0.1$ and Ra = 10^4 $\zeta = 0.5, \lambda = 0.25,$ ——— nanofluid, − − − − pure water

(Al₂O₃)				
$|\theta_{max}|_{nf} = 0.131632$ $|\theta_{max}|_{f} = 0.155703$	$|\theta_{max}|_{nf} = 0.130636$ $|\theta_{max}|_{f} = 0.157214$	$|\theta_{max}|_{nf} = 0.126945$ $|\theta_{max}|_{f} = 0.152352$	$|\theta_{max}|_{nf} = 0.130639$ $|\theta_{max}|_{f} = 0.157211$	$|\theta_{max}|_{nf} = 0.131633$ $|\theta_{max}|_{f} = 0.158264$
(Ag)				
$|\theta_{max}|_{nf} = 0.126134$ $|\theta_{max}|_{f} = 0.155703$	$|\theta_{max}|_{nf} = 0.125232$ $|\theta_{max}|_{f} = 0.157214$	$|\theta_{max}|_{nf} = 0.122123$ $|\theta_{max}|_{f} = 0.152352$	$|\theta_{max}|_{nf} = 0.125237$ $|\theta_{max}|_{f} = 0.157211$	$|\theta_{max}|_{nf} = 0.126135$ $|\theta_{max}|_{f} = 0.158264$
(TiO₂)				
$|\theta_{max}|_{nf} = 0.136294$ $|\theta_{max}|_{f} = 0.155703$	$|\theta_{max}|_{nf} = 0.135062$ $|\theta_{max}|_{f} = 0.157214$	$|\theta_{max}|_{nf} = 0.131025$ $|\theta_{max}|_{f} = 0.152352$	$|\theta_{max}|_{nf} = 0.134941$ $|\theta_{max}|_{f} = 0.157211$	$|\theta_{max}|_{nf} = 0.136145$ $|\theta_{max}|_{f} = 0.158264$

FIGURE 6 Isotherms for different value of ($\gamma = -30°, -15°, 0°, 15°, 30°$) for nanofluid (Al₂O₃, Ag and TiO₂) at $\Phi = 0.15$ and Ra = 10^6 $\zeta = 0.5, \lambda = 0.25,$ ——— nanofluid, − − − − pure water

FIGURE 7 Isotherms for different value of ($\gamma = -30°, -15°, 0°, 15°, 30°$) for nanofluid (Al$_2O_3$, Ag and TiO$_2$) at $\Phi = 0.2$ and Ra $= 10^7$ $\zeta = 0.5, \lambda = 0.25$, ——— nanofluid, _ _ _ _ pure water
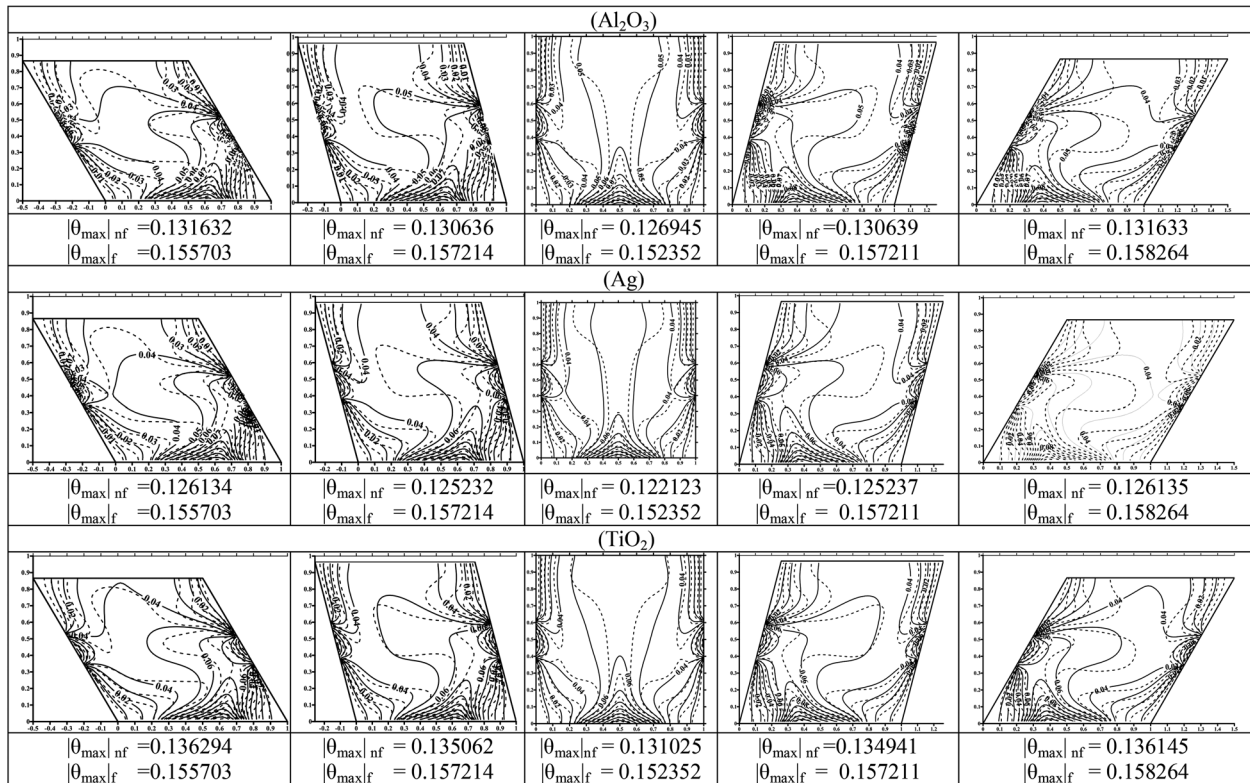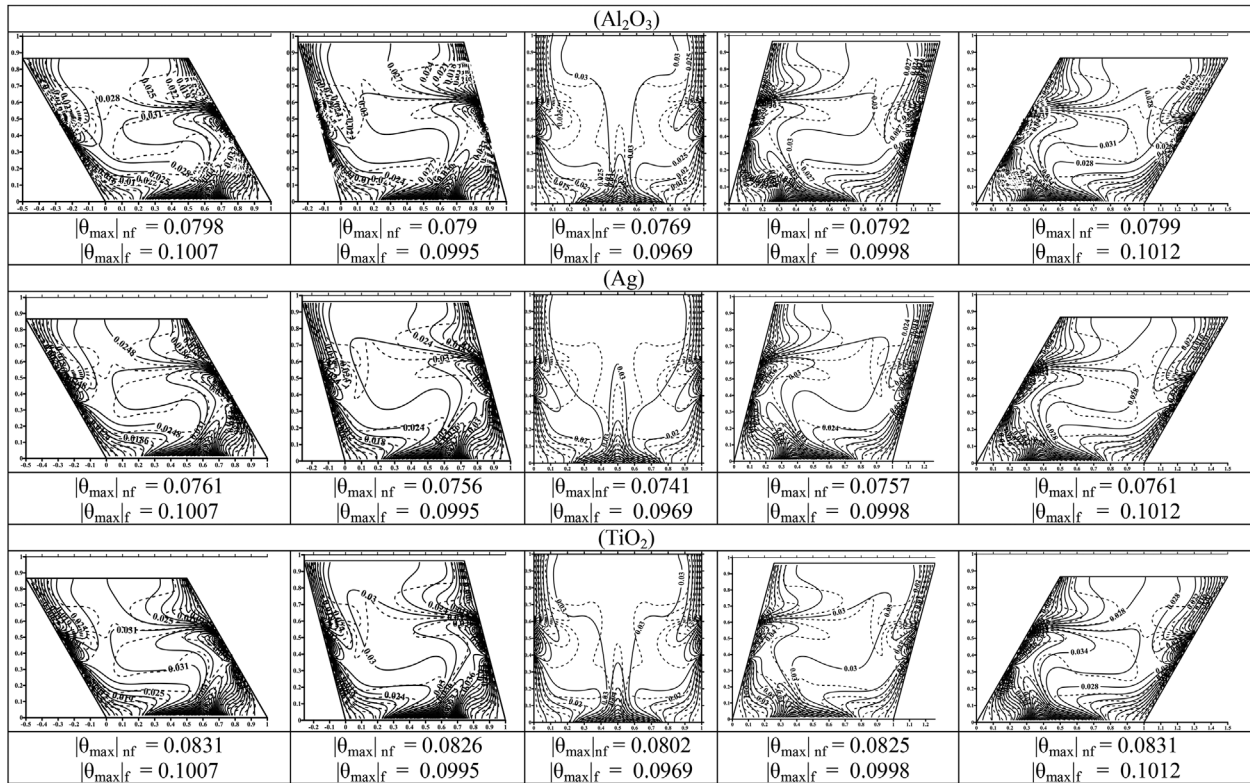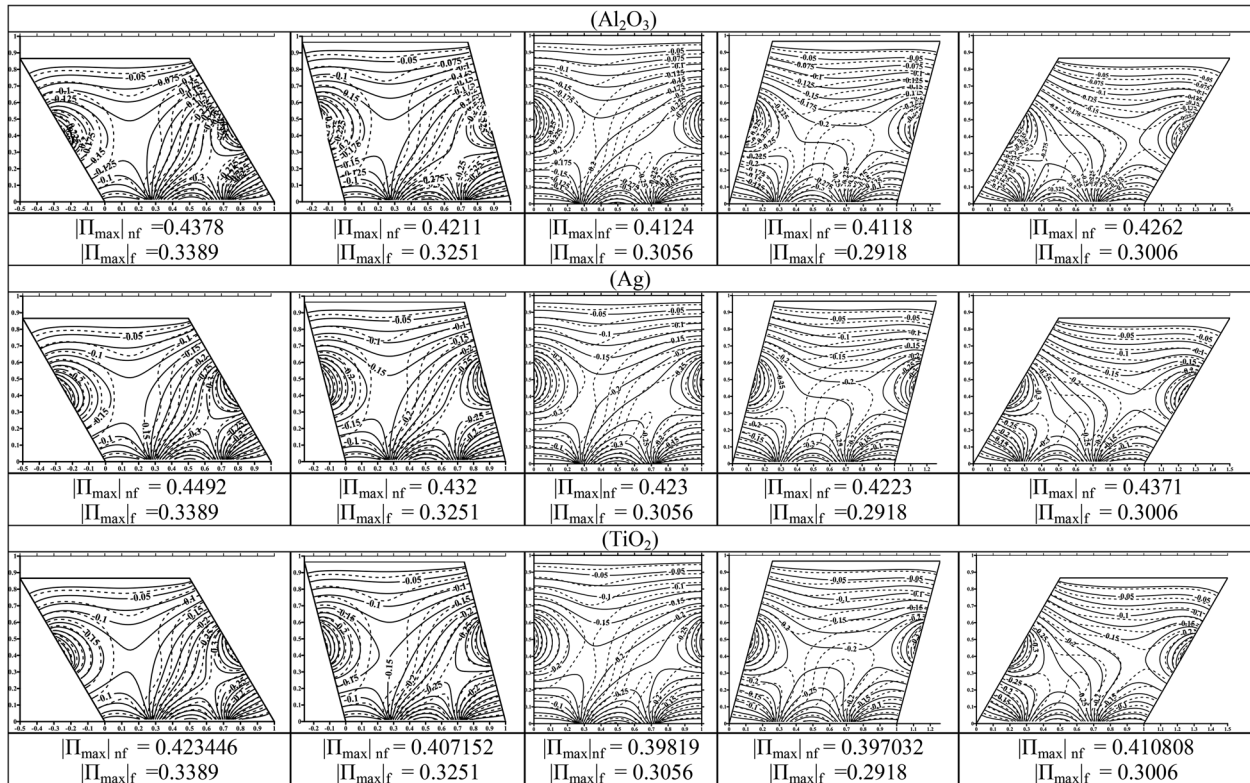

FIGURE 8 Heatfunction for different value of ($\gamma = -30°, -15°, 0°, 15°, 30°$) for nanofluid (Al$_2O_3$, Ag and TiO$_2$) at $\Phi = 0.1$ and Ra $= 10^4$ $\zeta = 0.5, \lambda = 0.25$, ——— nanofluid, _ _ _ _ pure water
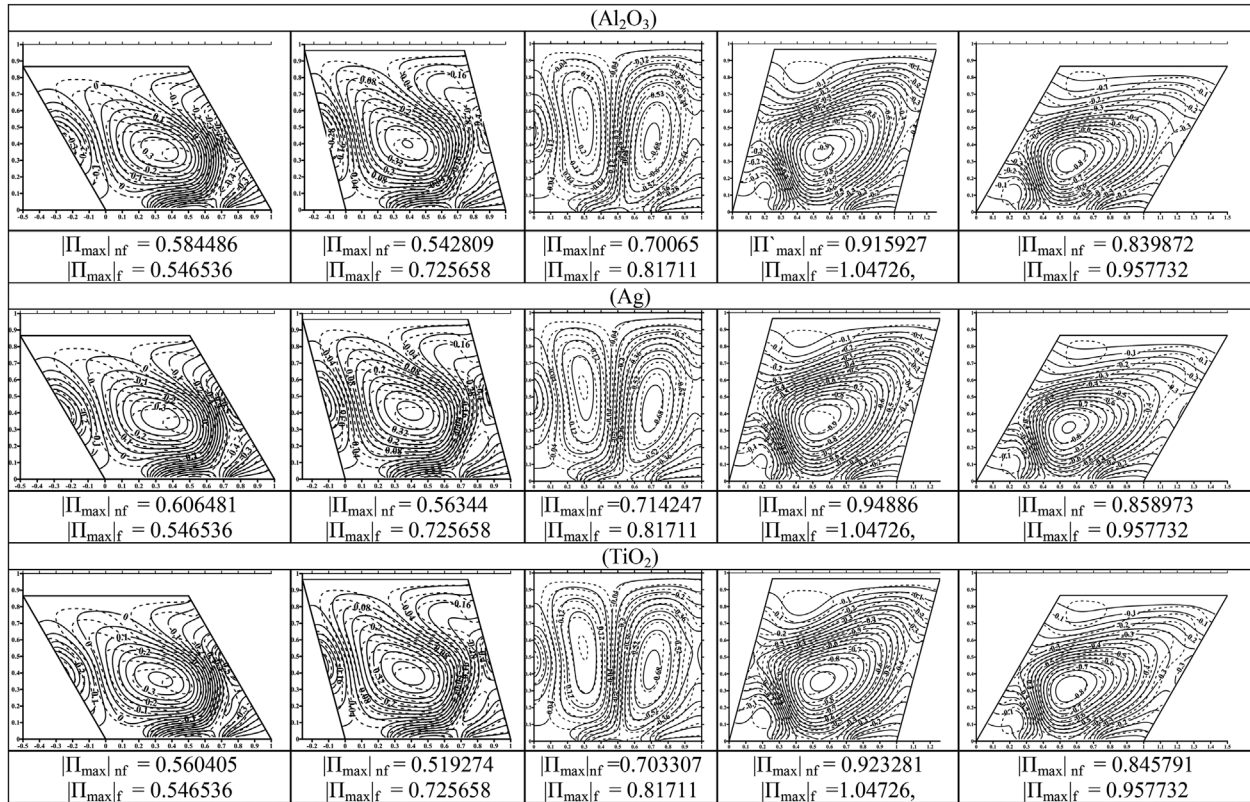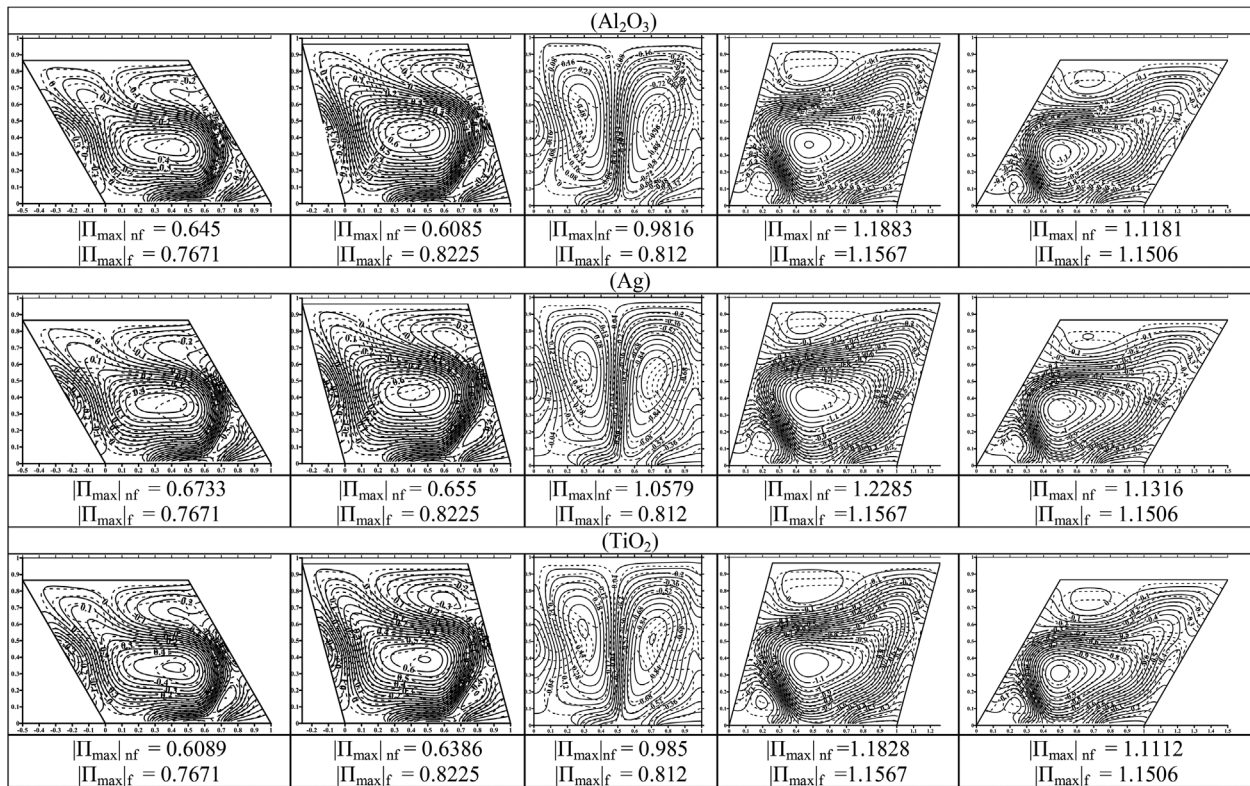
(Al₂O₃)				
$|\Pi_{max}|_{nf} = 0.584486$ $|\Pi_{max}|_f = 0.546536$	$|\Pi_{max}|_{nf} = 0.542809$ $|\Pi_{max}|_f = 0.725658$	$|\Pi_{max}|_{nf} = 0.70065$ $|\Pi_{max}|_f = 0.81711$	$|\Pi^`_{max}|_{nf} = 0.915927$ $|\Pi_{max}|_f = 1.04726,$	$|\Pi_{max}|_{nf} = 0.839872$ $|\Pi_{max}|_f = 0.957732$
(Ag)				
$|\Pi_{max}|_{nf} = 0.606481$ $|\Pi_{max}|_f = 0.546536$	$|\Pi_{max}|_{nf} = 0.56344$ $|\Pi_{max}|_f = 0.725658$	$|\Pi_{max}|_{nf} = 0.714247$ $|\Pi_{max}|_f = 0.81711$	$|\Pi_{max}|_{nf} = 0.94886$ $|\Pi_{max}|_f = 1.04726,$	$|\Pi_{max}|_{nf} = 0.858973$ $|\Pi_{max}|_f = 0.957732$
(TiO₂)				
$|\Pi_{max}|_{nf} = 0.560405$ $|\Pi_{max}|_f = 0.546536$	$|\Pi_{max}|_{nf} = 0.519274$ $|\Pi_{max}|_f = 0.725658$	$|\Pi_{max}|_{nf} = 0.703307$ $|\Pi_{max}|_f = 0.81711$	$|\Pi_{max}|_{nf} = 0.923281$ $|\Pi_{max}|_f = 1.04726,$	$|\Pi_{max}|_{nf} = 0.845791$ $|\Pi_{max}|_f = 0.957732$

FIGURE 9 Heatfunction for different value of ($\gamma = -30°, -15°, 0°, 15°, 30°$) for nanofluid (Al₂O₃, Ag and TiO₂) at $\Phi = 0.15$ and Ra = 10^6 $\zeta = 0.5$, $\lambda = 0.25$, ——— nanofluid, _ _ _ pure water

(Al₂O₃)				
$|\Pi_{max}|_{nf} = 0.645$ $|\Pi_{max}|_f = 0.7671$	$|\Pi_{max}|_{nf} = 0.6085$ $|\Pi_{max}|_f = 0.8225$	$|\Pi_{max}|_{nf} = 0.9816$ $|\Pi_{max}|_f = 0.812$	$|\Pi_{max}|_{nf} = 1.1883$ $|\Pi_{max}|_f = 1.1567$	$|\Pi_{max}|_{nf} = 1.1181$ $|\Pi_{max}|_f = 1.1506$
(Ag)				
$|\Pi_{max}|_{nf} = 0.6733$ $|\Pi_{max}|_f = 0.7671$	$|\Pi_{max}|_{nf} = 0.655$ $|\Pi_{max}|_f = 0.8225$	$|\Pi_{max}|_{nf} = 1.0579$ $|\Pi_{max}|_f = 0.812$	$|\Pi_{max}|_{nf} = 1.2285$ $|\Pi_{max}|_f = 1.1567$	$|\Pi_{max}|_{nf} = 1.1316$ $|\Pi_{max}|_f = 1.1506$
(TiO₂)				
$|\Pi_{max}|_{nf} = 0.6089$ $|\Pi_{max}|_f = 0.7671$	$|\Pi_{max}|_{nf} = 0.6386$ $|\Pi_{max}|_f = 0.8225$	$|\Pi_{max}|_{nf} = 0.985$ $|\Pi_{max}|_f = 0.812$	$|\Pi_{max}|_{nf} = 1.1828$ $|\Pi_{max}|_f = 1.1567$	$|\Pi_{max}|_{nf} = 1.1112$ $|\Pi_{max}|_f = 1.1506$

FIGURE 10 Heatfunction for different value of ($\gamma = -30°, -15°, 0°, 15°, 30°$) for nanofluid (Al₂O₃, Ag, and TiO₂) at $\Phi = 0.2$ and Ra = 10^7 $\zeta = 0.5$, $\lambda = 0.25$, ——— nanofluid, _ _ _ pure water
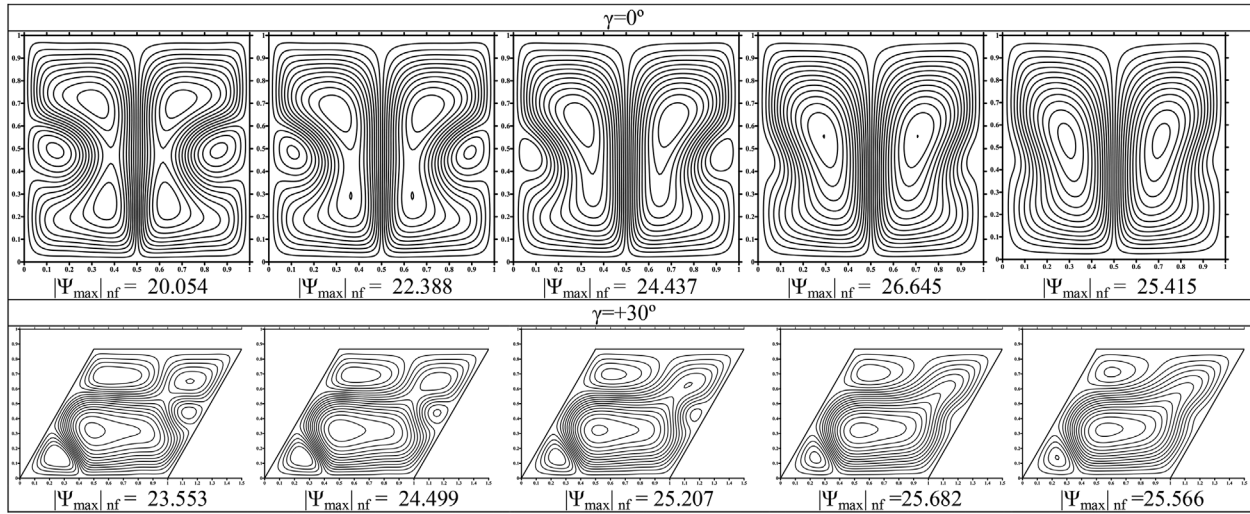
FIGURE 11 The effect of nanoparticles on the nanofluid stability (Streamfunction, $\Phi = 0, 0.05, 0.1, 0.15, 0.2$ respectively) for Al_2O_3 at Ra $= 10^7$, $\zeta = 0.5$, $\lambda = 0.25$
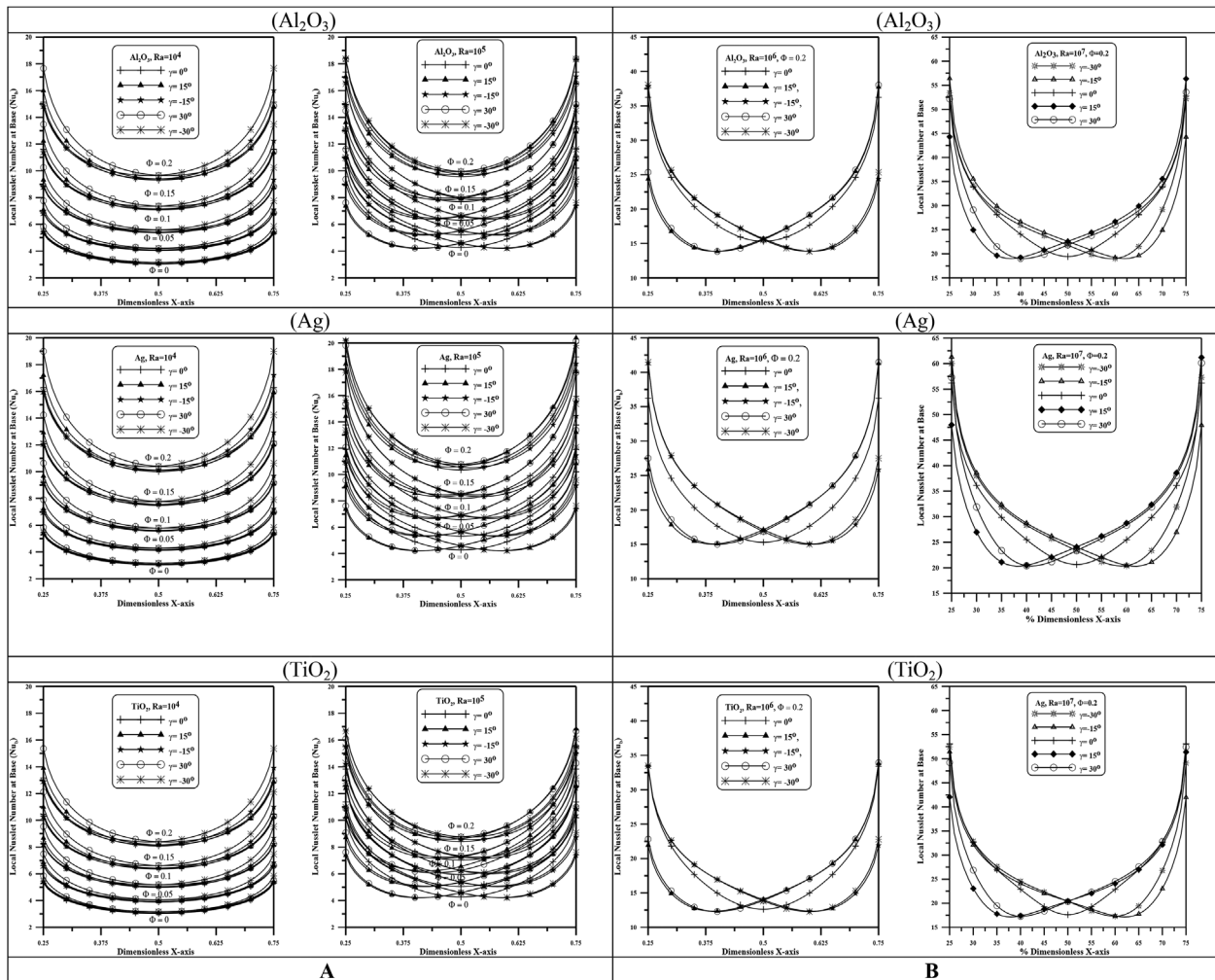

FIGURE 12 The local Nusselt number on the heat source at the base for (A) all Φ and Ra $= 10^4$-10^5, (B) for $\Phi = 0.2$ and Ra $= 10^6$-10^7
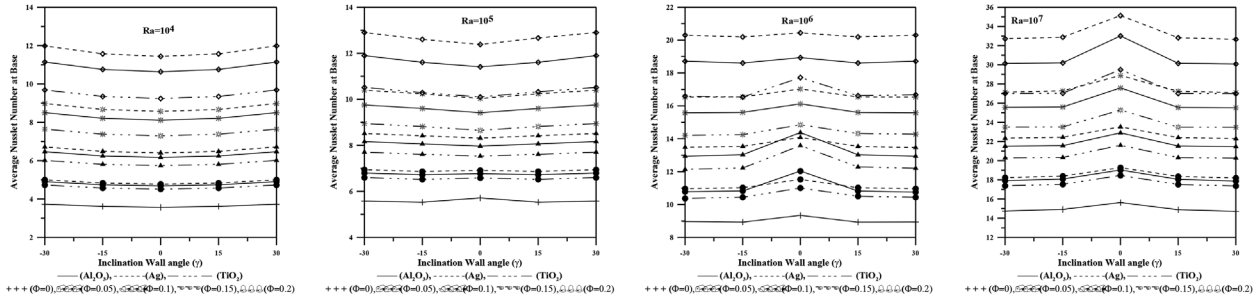
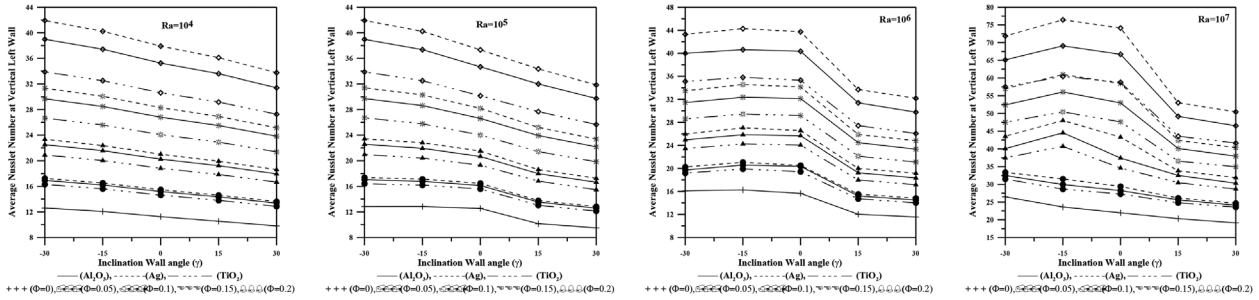**FIGURE 13** The average Nusselt number on the heat source at the base wall

FIGURE 14 The average Nusselt number on the heat source at the Left vertical

fluid at the top wall reverse its flow direction towards the hot regions and replaces by more warm fluid layer, therefore; the enclosure fills by big eddy and a small one in the right bottom corner due to its slop the right wall toward the bottom wall and enforced isoflux boundary conditions. As γ increases the small eddy grows and two symmetrical rotating eddies occupied the enclosure at ($\gamma = 0°$) due to symmetrical boundary condition and analogous image with opposite direction can noticed at ($\gamma = 15°$ and $30°$). The notice point that the value of stream function has a maximum value at ($\gamma = \pm30°$) for
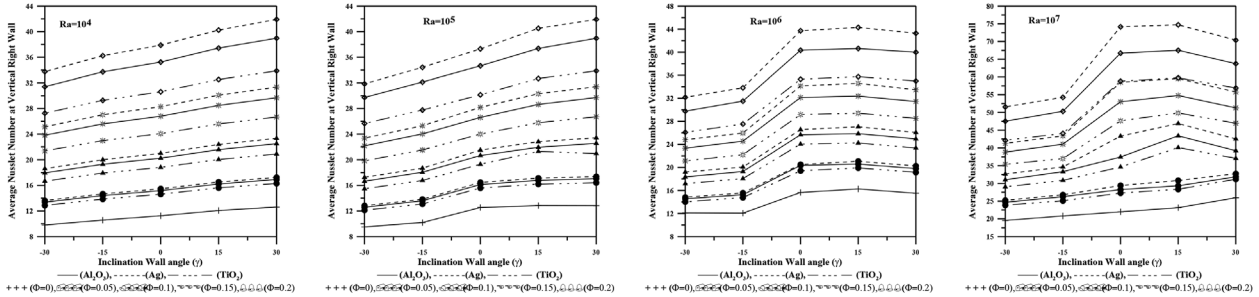
FIGURE 15 The average Nusselt number on the heat source at the right vertical

TABLE 4 Maximum stream function values for different value of ($\gamma = -30°, -15°, 0°, 15°, 30°$) for nanofluid ($Al_2O_3$, Ag, and TiO_2) at $\Phi = 0.1$

Γ	$\%\Psi_{max}|_{\Phi = 0.1}$ $Ra = 10^5$				$\%\Psi_{max}|_{\Phi = 0.1}$ $Ra = 10^6$				$\%\Psi_{max}|_{\Phi = 0.1}$ $Ra = 10^7$			
	Pure water	Al_2O_3	Ag	TiO_2	Pure water	Al_2O_3	Ag	TiO_2	Pure water	Al_2O_3	Ag	TiO_2
30	572	970	956	945	1534	3311	3271	3131	2895	6727	6578	6335
15	602	1093	1080	1136	1703	3839	3829	3637	3007	7890	7776	7393
0	608	994	981	969	2080	4088	3861	3911	3663	9702	10816	9037
−15	602	1093	1080	1061	1704	3841	3832	3635	3022	7907	7789	7407
−30	572	971	957	945	1515	3311	3235	3128	2901	6743	6592	6343

TABLE 5 Maximum stream function values for different value of ($\gamma = -30°, -15°, 0°, 15°, 30°$) for nanofluid ($Al_2O_3$, Ag, and TiO_2) at $Ra = 10^6$

γ	$\%\Psi_{max}\|_{\Phi=0.05}$ $Ra=10^6$			$\%\Psi_{max}\|_{\Phi=0.1}$ $Ra=10^6$			$\%\Psi_{max}\|_{\Phi=0.15}$ $Ra=10^6$			$\%\Psi_{max}\|_{\Phi=0.2}$ $Ra=10^6$		
	Al_2O_3	Ag	TiO_2	Al_2O_3	Ag	TiO_2	Al_2O_3	Ag	TiO_2	Al_2O_3	Ag	TiO_2
30	−2	1	−2	−2	2	−4	−5	2	−6	−10	−1	−10
15	−1	2	−1	−3	3	−4	−7	1	−8	−14	−3	−14
0	−3	−5	−7	−11	−10	−11	−21	−17	−21	−30	−24	−27
−15	−1	2	−1	−3	3	−4	−7	1	−8	−14	−3	−14
−30	−2	1	−1	−1	2	−3	−3	3	−5	−9	0	−10

TABLE 6 Maximum isotherms values for different value of ($\gamma = -30°, -15°, 0°, 15°, 30°$) for nanofluid ($Al_2O_3$, Ag, and TiO_2) at $\Phi = 0.05$ & $\Phi = 0.2$

γ	$\%\theta_{max}\|_{\Phi=0.05}$ $Ra=10^5$				$\%\theta_{max}\|_{\Phi=0.05}$ $Ra=10^6$				$\%\theta_{max}\|_{\Phi=0.05}$ $Ra=10^7$			
	Pure water	Al_2O_3	Ag	TiO_2	Pure water	Al_2O_3	Ag	TiO_2	Pure water	Al_2O_3	Ag	TiO_2
30	−26	−20	−21	−21	−50	−46	−46	−46	−69	−66	−66	−66
15	−27	−22	−22	−22	−52	−48	−48	−49	−70	−67	−67	−67
0	−29	−23	−23	−23	−54	−50	−50	−51	−71	−68	−68	−69
−15	−27	−22	−22	−22	−52	−48	−48	−48	−70	−67	−67	−67
−30	−26	−20	−21	−21	−51	−46	−46	−46	−69	−66	−66	−66

γ	$\%\theta_{max}\|_{\Phi=0.2}$ $Ra=10^5$				$\%\theta_{max}\|_{\Phi=0.2}$ $Ra=10^6$				$\%\theta_{max}\|_{\Phi=0.2}$ $Ra=10^7$			
	Pure Water	Al_2O_3	Ag	TiO_2	Pure Water	Al_2O_3	Ag	TiO_2	Pure Water	Al_2O_3	Ag	TiO_2
30	−26	−4	−4	−5	−50	−31	−31	−32	−69	−55	−55	−57
15	−27	−4	−5	−5	−52	−33	−33	−34	−70	−57	−57	−58
0	−29	−3	−4	−4	−54	−35	−35	−37	−71	−59	−58	−60
−15	−27	−4	−5	−5	−52	−33	−33	−34	−70	−57	−57	−58
−30	−26	−4	−4	−5	−51	−31	−31	−32	−69	−55	−55	−57

TABLE 7 Maximum isotherms values for different value of ($\gamma = -30°, -15°, 0°, 15°, 30°$) for nanofluid ($Al_2O_3$, Ag, and TiO_2) at $Ra = 10^4$ & $Ra = 10^7$

γ	$\%\theta_{max}\|_{\Phi=0.05}$ $Ra=10^4$			$\%\theta_{max}\|_{\Phi=0.1}$ $Ra=10^4$			$\%\theta_{max}\|_{\Phi=0.15}$ $Ra=10^4$			$\%\theta_{max}\|_{\Phi=0.2}$ $Ra=10^4$		
	Al_2O_3	Ag	TiO_2	Al_2O_3	Ag	TiO_2	Al_2O_3	Ag	TiO_2	Al_2O_3	Ag	TiO_2
30	−14	−15	−12	−26	−28	−23	−36	−38	−33	−45	−47	−41
15	−14	−15	−12	−26	−28	−23	−36	−38	−32	−45	−47	−41
0	−14	−15	−13	−26	−28	−23	−36	−39	−33	−45	−48	−41
−15	−14	−15	−12	−26	−28	−23	−36	−38	−32	−45	−47	−41
−30	−14	−15	−12	−26	−28	−23	−36	−38	−33	−45	−47	−41

γ	$\%\theta_{max}\|_{\Phi=0.05}$ $Ra=10^7$			$\%\theta_{max}\|_{\Phi=0.1}$ $Ra=10^7$			$\%\theta_{max}\|_{\Phi=0.15}$ $Ra=10^7$			$\%\theta_{max}\|_{\Phi=0.2}$ $Ra=10^7$		
	Al_2O_3	Ag	TiO_2	Al_2O_3	Ag	TiO_2	Al_2O_3	Ag	TiO_2	Al_2O_3	Ag	TiO_2
30	−7	−8	−5	−12	−14	−10	−15	−17	−14	−22	−25	−18
15	−6	−7	−5	−12	−14	−10	−14	−17	−14	−21	−25	−18
0	−6	−7	−5	−11	−12	−9	−14	−16	−13	−21	−24	−18
−15	−6	−7	−6	−11	−13	−10	−14	−17	−14	−21	−25	−18
−30	−6	−7	−5	−12	−14	−10	−14	−17	−14	−21	−25	−18

TABLE 8 Maximum heatfunction values for different value of ($\gamma = -30°, -15°, 0°, 15°, 30°$) for nanofluid (Al$_2O_3$, Ag, and TiO$_2$) at $\Phi = 0.1$

γ	%Π_{max}|$\Phi = 0.1$ Ra $= 10^5$				%Π_{max}|$\Phi = 0.1$ Ra $= 10^6$				%Π_{max}|$\Phi = 0.1$ Ra $= 10^7$			
	Pure water	Al$_2$O$_3$	Ag	TiO$_2$	Pure water	Al$_2$O$_3$	Ag	TiO$_2$	Pure water	Al$_2$O$_3$	Ag	TiO$_2$
30	90	8	8	14	218	108	105	116	282	167	159	177
15	121	23	23	27	259	134	134	144	296	191	186	201
0	68	7	7	12	167	81	75	88	165	133	158	138
−15	16	13	13	14	123	31	31	39	153	78	75	87
−30	19	14	14	15	61	19	19	20	126	43	37	52

TABLE 9 Maximum heatfunction values for different value of ($\gamma = -30°, -15°, 0°, 15°, 30°$) for nanofluid (Al$_2O_3$, Ag, and TiO$_2$) at Ra $= 10^4$

γ	%Π_{max}|$\Phi = 0.5$ Ra $= 10^4$			%Π_{max}|$\Phi = 0.1$ Ra $= 10^4$			%Π_{max}|$\Phi = 0.15$ Ra $= 10^4$			%Π_{max}|$\Phi = 0.2$ Ra $= 10^4$		
	Al$_2$O$_3$	Ag	TiO$_2$	Al$_2$O$_3$	Ag	TiO$_2$	Al$_2$O$_3$	Ag	TiO$_2$	Al$_2$O$_3$	Ag	TiO$_2$
30	20	21	18	41	45	36	65	71	56	91	101	78
15	20	21	17	41	44	36	64	70	55	89	99	77
0	16	17	14	34	38	30	56	62	48	80	89	68
−15	13	14	11	29	32	25	48	54	41	71	80	60
−30	12	14	11	29	32	24	48	54	41	70	79	59

nanofluid while for pure water maximum value observe at ($\gamma = \pm15°$). Also the Ag-water nanofluid has a maximum value of stream function while Al$_2$O$_3$ has a minimum value of stream function for all inclination angles, due to the increase in thermal conductivity causes the increase in circulation strength. The values of stream function for nanofluid are less than for pure water (?). For Ag-water ($|\Psi_{max}|$) $= 0.392$ at (Ra $= 10^4$) and ($\gamma = \pm30°$) and for pure water ($|\Psi_{max}| = 0.82$ at (Ra $= 10^4$) and ($\gamma = \pm15°$). As the Rayleigh number and volume fraction increase (Ra $= 10^6$) and ($\Phi = 0.15$) in Figure 3 leads to increase both intensity of stream function and size of vortex due to the influence of buoyancy force increasing over computation viscous force. It is a marked increase in the values of the maximum stream function for both pure water and nanofluid. Also Ag-water nanofluid has maximum intensity of stream function compared with other types of nanofluid TiO$_2$-water nanofluid and Al$_2$O$_3$-water nanofluids. The effect of inclination angle is clear in both magnitude and streamlines behavior. Maximum values of stream intensity achieved in the same skew angle ($\gamma = \pm15°$) for water and nanofluid in this case. For Ag-water ($|\Psi_{max}|_{nf} = 15.0423$) and for pure water ($|\Psi_{max}|_f = 14.7926$). Figure 4 represents the stream function contour at (Ra $= 10^7$) and ($\Phi = 0.2$) for three types of nanofluid with a range of skew angles ($-30° \le \gamma \le 30°$). As expected recently, as Rayleigh number increases and volume fraction increases, the flow rotation increase causes the values of stream function increasingly remarkably for nanofluid and pure water. As a sample for Ag-water ($|\Psi_{max}|_{nf} = 0.265$) and for pure water ($|\Psi_{max}|_f = 0.533$) at ($\gamma = 0$) and (Ra $= 10^4$) when Rayleigh increases at the same conditions ($|\Psi_{max}|_{nf} = 29.198$) and for pure water ($|\Psi_{max}|_f = 20.054$) at (Ra $= 10^7$). As evident in the shape of vortexes transforms from the circular form to ellipsoid form. It can clearly observe that the coincidence of streamlines between nanofluid and pure water was vanishing as the solid volume fraction increases. As the volume fraction of nanofluids becomes ($\Phi = 0.2$) the strength of vortexes increase due to increase of thermal conductivity. It can see that the behavior of fluid flow affected by nanofluids. Vortexes of pure water are greater than for nanofluid especially at the higher Rayleigh number and volume fraction because the certain streamline diameter of the water vortex is greater than that for nanofluids at the specific magnitude of stream function as described in [35].

5.2 | Effect of enclosure skew angle and Rayleigh number on thermal field

Figure 5 shows isothermal lines for three types of nanofluids (Al$_2$O$_3$-water), (Ag-water) and (TiO$_2$-water), different skew angles ($-30°, -15°, 0°, 15°, 30°$), at Rayleigh number (Ra $= 10^4$) and volume fraction ($\Phi = 0.1$). It is clear that the isothermal lines are clustering sharply near three discrete isle regions. The temperature gradient decreases from the bottom

wall contain large discrete isoflux toward the adiabatic top wall with significant large gradient near the isoflux heating regions. At this Rayleigh number conduction heat transfer mode is dominant. Isothermal lines for three types of nanofluids and base fluid display alike behavior near the bottom and side walls, with slim difference near the top wall. It is remarkable to notice that thermal boundary layer thickness for the three types of nanofluid is greater than for base fluid due to greater viscosity and less fluid movement. Also it is found that dimensionless temperature for different types of nanofluids are less than that for base fluid at all skew angles. For example at $(\gamma = 0^o)$ $|\theta_{max}|_{Ag} = 0.2393$, $|\theta_{max}|_{Al_2O_2} = 0.2454$, $|\theta_{max}|_{TiO_2} = 0.254184$ and for base fluid $|\theta_{max}|_f = 0.3294$, also when the. Also, we can notice that when the angle of inclination has positive or negative value dimensionless temperature less than on $(\gamma = 0^o)$, for example for Ag-water nanofluid $|\theta_{max}|_{\gamma = 0^o} = 0.2393$, $|\theta_{max}|_{\gamma = \mp 15^o} = 0.23694$, $|\theta_{max}|_{\gamma = \mp 30^o} = 0.2305$, while for base fluid $|\theta_{max}|_{\gamma = 0^o} = 0.3294$, $|\theta_{max}|_{\gamma = \mp 15^o} = 0.3252$, $|\theta_{max}|_{\gamma = \mp 30^o} = 0.3165.?$. Figure 6 shows the same variables which are studied in Figure 5 except the Rayleigh number are taken Ra = 10^6 and volume fraction ($\Phi = 0.15$). As Rayleigh number increased and volume fraction increase, the influence of convection is increasing within all the cavity due to enhanced buoyancy force. The temperature distribution near the discrete isoflux regions tend to grow thermal boundary layer inside the enclosure. The isothermal lines change significantly with increasing Rayleigh indicates that the connection is the dominating heat transfer mechanism in the cavity. Due to enhance convection entire the enclosure the isothermal lines are more disturbance for both nano and base fluid. At $\gamma = 0^o$ the isothermal lines have symmetrical contour for all types of nanofluids and base fluid which have values for Al_2O_3 $|\theta_{max}|_{\gamma = 0^o} = 0.126945$ for Ag $|\theta_{max}|_{\gamma = 0^o} = 0.122123$ and for TiO_2 $|\theta_{max}|_{\gamma = 0^o} = 0.131025$ while in the water $|\theta_{max}|_{\gamma = 0^o} = 0.152352$. From this result, it correct to say, that addition nanoparticle decrease the maximum dimensionless temperature, which is referred to improve the cooling system entire the enclosure. As the inclination angle change with positive or negative values the dimensionless temperature increase for nanofluid and base fluid and which has a maximum value for nanofluid art $\gamma = \pm 30^o$ $|\theta_{max}|_{Al_2O_3} = 0.131632$, $|\theta_{max}|_{Ag} = 0.126234$, $|\theta_{max}|_{TiO_2} = 0.136294$, while for base fluid at $\gamma = \pm 15$ $|\theta_{max}|_{water} = 0.157214$.

Figure 7 represents the isotherms for different value of $\gamma = 0^o, \pm 15^o, \pm 30^o$, for nanofluids Al_2O_3, Ag and TiO_2 at volume fraction $\Phi = 0.2$ and Ra = 10^7. At high Rayleigh number the isotherms have considerable twisting existence and concentrated at discrete heating region and cold wall, since the thermally-made buoyancy force is enhanced. The addition of nanoparticle to water, enhance the thermal conductivity, therefore the energy transport improved and performance of heat transfer increase. This fact can observe in results the maximum dimensionless temperature for Al_2O_3- nanofluid is $|\theta_{max}|_{\gamma = 0^o} = 0.0769$ for Ag-nanofluid $|\theta_{max}|_{\gamma = 0^o} = 0.0741$ for TiO_2 $|\theta_{max}|_{\gamma = 0^o} = 0.0802$ and for water $|\theta_{max}|_{\gamma = 0^o} = 0.0969$, the less value for Ag-nanofluid because has higher thermal conductivity. The irregularity of the isotherms is clear for the vertical cavity $(\gamma = 0^o)$ with symmetric shapes for all types of nanofluids and base fluid. As the cavity skew angle changes, the symmetrical shape vanish and the dimensionless temperature increase slightly. For Al_2O_3 $|\theta_{max}|_{\gamma = 0^o} = 0.0769$, $|\theta_{max}|_{\gamma = \mp 15^o} = 0.0792$, $|\theta_{max}|_{\gamma = \pm 30^o} = 0.0799$, for Ag-nanofluid $|\theta_{max}|_{\gamma = 0^o} = 0.0741$, $|\theta_{max}|_{\gamma = \pm 15^o} = 0.0756$, $|\theta_{max}|_{\gamma = \pm 30^o} = 0.0761$, for TiO_2-nanofluid $|\theta_{max}|_{\gamma = 0^o} = 0.0802$, $|\theta_{max}|_{\gamma = \pm 15^o} = 0.0826$, $|\theta_{max}|_{\gamma = \pm 30^o} = 0.0831$, for water $|\theta_{max}|_{\gamma = 0^o} = 0.0969$, $|\theta_{max}|_{\gamma = \pm 15^o} = 0.0995$, $|\theta_{max}|_{\gamma = \pm 30^o} = 0.1007$. A result, the skew angle enhances heat transfer at low Rayleigh number (Ra = 10^4), while depressed heat at high Rayleigh number (10^6 and 10^7).

5.3 | Effect of enclosure skew angle and Rayleigh number on heatlines contours

The dimensionless temperature provide an outlook about the temperature gradient inside the enclosure, while, heatlines offer a good overview about heat transfer strength and tendency. Positive heat function ($+\Pi$) refers to anti-clockwise fluid-heat transfer flow, while a negative sign ($-\Pi$) denote clockwise fluid-heat transfer flow. Π_{max} signify the best heat function, therefore this value is necessary to describe the maximum variation of heat circulation. Figure 8 shows the heart function for different value of the skew angle ($\gamma = 0^o, \gamma = \pm 15, \gamma = \pm 30$) and for three types of nanofluids (Al_2O_3, Ag and TiO_2) at volume fraction $\Phi = 0.1$ and Ra = 10^4. The result show that the additive nanoparticles increase the heart function, the value of the heat function for base fluid at vertical enclosure $(\gamma = 0^o)$ is ($\Pi_{max} = 0.3056$) while for Al_2O_3 ($\Pi_{max} = 0.4124$), for Ag ($\Pi_{max} = 0.423$), for TiO_2 ($\Pi_{max} = 0.39819$), also the optimal value is found for Ag, since the Ag has an optimal thermal conductivity. As the inclination angle increase ($\gamma = +15^o, +30^o$), the heat function, increase for both base fluid and three types of nanofluids. As the angle of inclination decrease ($\gamma = -15^o$) the value of the heat function, decrease and has a minimum value of the heat function for base and all types of nanofluid. When the angle of inclination has value ($\gamma = -30^o$), the heat function increase. This behavior is due to the conduction heat transfer in the natural convection when (Ra = 10^4) is dominant. As the Rayleigh number increase (Ra = 10^6) and volume fraction increase ($\Phi = 0.15$) as in Figure 9

for the same other parameters the values of heat function, increase at ($\gamma = 0^0$) for Al_2O_3 nanofluid from ($\Pi_{max} = 0.4124$), for Ag ($\Pi_{max} = 0.423$), for TiO_2 ($\Pi_{max} = 0.39819$) and for water ($\Pi_{max} = 0.3056$) to ($\Pi_{max} = 0.70065$) for Al_2O_3, ($\Pi_{max} = 0.714247$) for Ag, ($\Pi_{max} = 0.703307$) for TiO_2, ($\Pi_{max} = 0.81711$) for water. This rise because convection is dominant in the natural convection. When skew angle increase from ($\gamma = 0^o$) to ($\gamma = +15^o$) the magnitude of the heat function decreases for nano and base fluid. But at ($\gamma = +30^o$) the heat function increase slowly. On the other hand, when the skew angle decreases, which has a negative sign ($\gamma = -15^o$), the heat function, increase significantly for Al_2O_3 from ($\Pi_{max} = 0.714247$) to ($\Pi_{max} = 0.915927$), for Ag from ($\Pi_{max} = 0.714247$) to ($\Pi_{max} = 0.94886$), for TiO_2 from ($\Pi_{max} = 0.703307$) to ($\Pi_{max} = 0.923281$) and for water from ($\Pi_{max} = 0.81711$) to ($\Pi_{max} = 1.04726$). An opposite manners present at ($\gamma = -30^o$) where the value of the heat function becomes for Al_2O_3 ($\Pi_{max} = 0.839872$). For Ag ($\Pi_{max} = 0.858973$), for TiO_2 ($\Pi_{max} = 0.845791$) and for water ($\Pi_{max} = 0.957732$). As increasing Rayleigh number ($Ra = 10^7$) and volume fraction ($\Phi = 0.2$) in Figure 10 which represent the heat function for three types of nanofluids Al_2O_3, Ag and TiO_2 and five skew angle ($\gamma = 0^o$, $\gamma = \pm15^o$, $\gamma = \pm30^o$). As expected the heat function, increase with increasing Rayleigh numbers and volume fraction increase for both nano and water fluid due to convection has major influence in natural convection heat transfer. Also the Ag nanofluid has maximum values of the heat function for different skew angle since it has higher thermal conductivity. The result display that the minimum value of the heat function for Al_2O_3 and Ag obtained at a skew angle ($\gamma = -15^o$) which has ($\Pi_{max} = 0.6085$) for Al_2O_3 and ($\Pi_{max} = 0.655$) for Ag while the minimum value of the heat function for TiO_2 and base fluid obtained at a skew angle ($\gamma = -30^o$) which has ($\Pi_{max} = 0.6089$) for TiO_2 nanofluid and ($\Pi_{max} = 0.7671$) for pure water. Also the result show that the maximum value of a heat function can be noticed at ($\gamma = -15^o$) for both nano and base fluid which has ($\Pi_{max} = 1.1883$) for Al_2O_3, ($\Pi_{max} = 1.2285$) for Ag, ($\Pi_{max} = 1.1828$) for TiO_2 and ($\Pi_{max} = 1.1567$) for water. It is important to note from the result of the heat function that the behavior and magnitude of heat function were significantly affected by Rayleigh number, the type of nanofluid and skew angle.

Figure 11 illustrates the effect of nanoparticles on the fluid stability for pure water and four volume fraction of Al_2O_3 nanofluid ($\Phi = 0.05, 0.1, 0.15$ and 0.2) at higher Rayleigh number ($Ra = 10^7$) at two skew angles ($\gamma = 0^o, 30^o$). For pure water the enclosure contains six eddies, three rotates with clockwise and the other three with anti-clockwise rotating. Four big eddies appear in every quarter of the enclosure and two small presents in the middle-side walls of the enclosure. This due to convection dominant the natural convection inside the enclosure. The addition of nanoparticles to the pure water increase viscosity force. The rise of the viscosity force reduction the fluid velocity, therefore, at a small volume fraction ($\Phi = 0.05, 0.1, 0.15$) makes the small eddies to vanish and big eddies to merge. Also the strength of eddies increase ($\Psi_{max})_{\Phi = 0} = 20.054$, ($\Psi_{max})_{\Phi = 0.05} = 22.388$, ($\Psi_{max})_{\Phi = 0.1} = 24.437$, ($\Psi_{max})_{\Psi = 0.15} = 26.645$, while at ($\Phi = 0.2$) the effect of increasing viscosity force appears, therefore the value of stream function decrease ($\Psi_{max})_{\Psi = 0.2} = 25.415$. At the skew angle ($\gamma = 30^o$) the value of stream function, increased for both base and nanofluid therefore it becomes ($\Psi_{max})_{\Psi = 0} = 23.553$, ($\Psi_{max})_{\Psi = 0.1} = 24.499$, ($\Psi_{max})_{\Psi = 0.15} = 25.682$, ($\Psi_{max})_{\Psi = 0.2} = 25.566$. It can be concluded from the results that the addition of nanoparticles to the pure fluids enhancing the stability of the nanofluid produce since the viscous force increased.

5.4 | Local and average Nusselt number

The irregularity of temperature distribution over the discrete isoflux existed in the components of electronic devices. The irregularity of surface temperature has an opposing influence on the life and functionality of this electronic components. Therefore, distribution of local and average Nusselt number along the surface heated isoflux located on the bottom and side walls is studied in Figures 12, 13, 14 and 15.

Figure 12A and B presents the local Nusselt number along the bottom heat source for three types of nanofluid and for all skew angles, the range of Rayleigh number ($Ra = 10^4, 10^5, 10^6, 10^7$), volume of fraction ($\Phi = 0, 0.05, 0.1, 0.15$ and 0.2). The results display that the local Nusselt number has a parabolic profile for both base and nanofluid. It can be seen that the local Nusselt number has maximum values at the two ends of discrete heat source and minimum value at the middle. This is due to that the temperature distribution on the surface of the discrete isoflux is not regular and has a minimum value wherever the temperature difference to the nearby flow is maximal. The results show that the local Nusselt number increase by increasing solid volume fraction of nanoparticles. Ag and Al_2O_3 water nanofluid have optimal values of local Nusselt number when compared with TiO_2-nanofluid. Table 1 displays that Ag has an optimum value of thermal conductivity ($k = 429$ W/m K), follow by Al_2O_3 has a thermal conductivity ($k = 40$ W/m K) and TiO_2 has the lowest value of thermal conductivity ($k = 8.9538$ W/m K). Also, it can be noticed that the maximum local Nusselt number appears at the skew angles ($\gamma = \pm30^o$), since higher area that exchange heat transfer. Figure 12B shows the local Nusselt

number along the bottom heat source at higher Rayleigh number (10^6, 10^7) and solid volume fraction ($\Phi = 0.2$) explains the influence of the skew angle on the nanofluid obviously. The results show that as the Rayleigh number increase the local Nusselt number increase since the convection effect. At a skew angle ($\gamma = 0^\circ$) the profile of a local Nusselt number is symmetrical and minimum local Nusselt number localized in the middle of heat source since the flow has minimum strength. As the skew angle increases or decreases than (0°) the minimum value of local Nusselt number shifted to the left or to right effected by wall inclination.

Figure 13 shows the distribution of the average Nusselt number along the bottom heat source with skew angles for three types of nanofluids Al_2O_3, Ag, TiO_2 and pure water at a different Rayleigh number. The result display that the average Nusselt number have a linear and symmetrical profile. As expected the average Nusselt number reaches its maximum value at a higher Rayleigh number (Ra = 10^7). This performance is due to the higher convection effect produces higher strength of circulation and higher energy transport inside the enclosure. Also Ag-water nanofluid has a maximum average Nusselt number and pure water has a minimum value of average Nusselt number for all Rayleigh number and skew angles because the effect of thermal conductivity. It can deduce that the skew angle has a slightest influence on the average Nusselt number. Figures 14 and 15 display the variation of the average Nusselt number on the heat source at the left and right sidewalls with skew angles for three types of nanofluids Al_2O_3, Ag, TiO_2 and pure water at a different Rayleigh number. It is observed that for left heat source the average Nusselt number slightly decreases as the skew angle increase at low Rayleigh number (10^4, 10^5). At high Rayleigh number (10^6, 10^7) the average Nusselt number linearly variation with the increase of the skew angle attaining a maximum at a specific angle followed by an abrupt decrease before reaching to the lowest value at ($\gamma = 30^\circ$). A reverse performance can be noticed in the right heat source. The vertical heat source having a maximum average Nusselt number because the cell adjacent the it have high volume and strength.

5.5 | Heat transfer correlations

Based upon the results from the present simulations, nine correlation equations of average Nusselt number along the length of heat source of bottom ($\overline{Nu}_b$), left ($\overline{Nu}_L$) and right ($\overline{Nu}_R$) walls have been predicted depending on variation in Rayleigh numbers, side wall inclination angles and void fraction for three types of nanofluids (Al_2O_3, Ag and TiO_2–water) by using least square method. These correlations can be presented as follows:

$$\text{For } -30^\circ \leq \gamma \leq +30^\circ, \ \ 0 \leq \Phi \leq 0.2 \ \text{ and } 10^4 \leq Ra \leq 10^7$$

$$\overline{Nu}_b = 4.575 + 1.21 \times 10^{-6}Ra + 40.98 \times \Phi + 1.76 \times 10^{-5} \times \Phi$$

$$Al_2O_3, \quad R = 0.944$$

$$\overline{Nu}_L = 9.989 + 8 \times 10^{-7} \times Ra + 110.441 \times \Phi - 0.088 \times \Phi$$

$$Al_2O_3, \quad R = 0.962$$

$$\overline{Nu}_R = 9.990 + 8.20 \times 10^{-7} \times Ra + 110.332 \times \Phi + 0.092 \times \Phi$$

$$Al_2O_3, \quad R = 0.961$$

$$\overline{Nu}_b = 4.333 + 1.25 \times 10^{-6} \times Ra + 47.366 \times \Phi + 1.01 \times 10^{-6} \times \Phi$$

$$Ag, \quad R = 0.943$$

$$\overline{Nu}_L = 9.609 + 8.54 \times 10^{-7} \times Ra + 124.356 \times \Phi - 0.094 \times \Phi$$

$$Ag, \quad R = 0.961$$

$$\overline{Nu}_R = 9.667 + 8.82 \times 10^{-7} \times Ra + 123.688 \times \Phi + 0.096 \times \Phi$$

$$Ag, \quad R = 0.959$$

$$\overline{Nu}_b = 4.757 + 1.18 \times 10^{-6} \times Ra + 33.363 \times \Phi - 7.9 \times 10^{-5} \times \Phi$$

$$TiO_2, \quad R = 0.941$$

$$\overline{Nu}_L = 10.308 + 8.12 \times 10^{-7} \times Ra + 89.742 \times \Phi - 0.083 \times \Phi$$

$$Ti0_2, \quad R = 0.958$$

$$\overline{Nu}_R = 10.254 + 8 \times 10^{-7} \times Ra + 90.283 \times \Phi + 0.086 \times \Phi$$

$$Ti0_2, \quad R = 0.956$$

To ensure that these nine approximation correlations are usable, the maximum correlation coefficient or the residual had been obtained for each equation as mentioned above. The minimum value of the maximum correlation coefficient (R) is 0.941, which means that these nine approximate correlations are very good for predicting the value of an average Nusselt number.

6 | CONCLUSION

This paper examined the visualization of heatlines on natural convection in a Parallelogrammic enclosure with three different types of nanofluids Al_2O_3-whether, Ag-water and TiO_2-water subjected to three discrete isoflux in several walls, one discrete isoflux in the left wall, second in the right wall and third in the bottom wall. The finite element method based on Chorin's algorithm was used to analyze non-dimensional continuity, momentum and energy equations simultaneously with defined boundary conditions. The parameters influence on the heat transfer performance of Rayleigh number, skew angle, kind of nanofluids, particle volume fraction, discrete isoflux are examined through stream function, isotherms, heat function, local and average Nusselt number. The valuable remarks can be deduced are listed below.

- At low Rayleigh number (Ra = 104), an important enhancement observed in the strength of stream function, isotherms and heatlines with increasing or decreasing skew angle than ($\gamma = 0o$). With increasing Rayleigh number (Ra = 106, 107) optimum value of stream function can see it at ($\gamma = \pm15$) while the optimum value of isotherms at ($\gamma = 0o$).
- The strength of a stream function, increase as the Rayleigh number increases for both base and nanofluids which causes decreased in the discrete isoflux maximum temperature.
- Maximum temperature of discrete isoflux decreases with increasing solid volume fraction specially at low Rayleigh number since the conduction heat transfer was dominant.
- Addition nanoparticles increase the stability of fluid due to increase viscosity force produced decreases in velocity of nanofluid.
- The local Nusselt number distribution along discrete heated isoflux has parabolic trend, in general the local Nusselt number increase as the Rayleigh number increases and solid volume fraction increases too.
- To calculate the average Nusselt number for three kinds of nanofluids, nine relationship have been established. This relationship is based on the studying results and computing by using least square method (the maximum correlation coefficient (R) is 0.941).
- Subjectively, the upgraded of heat transfer performance is found in all the three nanofluids contrasted with that of the pure water yet the accompanying general outcome has:

$$Nu_{Ag-water} > Nu_{Al_2O_3-water} > Nu_{TiO_2} > base\ fluid_{water}$$

CONFLICTS OF INTEREST
The authors declare that they have no conflict of interest

REFERENCES

[1] Bejan, A.: Convection Heat Transfer. third Ed., Wiley Hoboken. NJ (2004)
[2] Joudi, K.A., Hussein, I.A., Ferhan, A.A.: Computational model for the prism shaped storage solar collector with a right triangular cross section. Energy Convers. Manage. 45, 391–409 (2004)
[3] Chiang, H., Kleinstreuer, C.: Analysis of passive cooling in a vertical finite channel using a falling liquid-film and buoyancy-induced gas vapor flow. Int. J. Heat Mass Transf. 34, 1791–1798 (1991)

[4] Dayem, A.M.A.: Experimental and numerical performance of multi-effect condensation solar water distillation system. Energy 31, 2710–2717 (2006)

[5] Mistry Ganapathi-Subbu, H., Dey, S., Bishnoi, P., Catillo, J.L.: Modeling of transient natural convection heat transfer in electric oven. Appl. Therm. Eng. 26, 2448–2456 (2006)

[6] Payvar, P.: Laminar heat transfer in the oil grooves of a wet clutch. Int. J. Heat Mass Transf. 34, 1791–1798 (1991)

[7] Hesse, P.M., Teubner, M.D.: Heat exchanger in an attic space. Int. J. Heat Mass Transf. 45, 44925–4936 (2002)

[8] Kalaiselvan, S., Veerappan, V., Aaron, A.A., Iniyan, S,: Experimental and analytical investigation of solidification and melting characteristics of PCMs inside the cylindrical encapsulation. Int. J. Therm. Sci. 47, 858–874 (2008)

[9] Wang, S.M., Faghri, A., Bergman, T.L.: A comprehensive numerical model for melting with natural convection. Int. J. Heat Mass Transf. 53, 1986–2000 (2010)

[10] Sheikholeslami, M., Gorji-Bandpy, M.: Free convection of ferrofluid in a cavity heated from below in the presence of an external magnetic field. Powder Technol. 256, 490–498 (2014)

[11] Zekeriya, A. and Seda, K.: Natural convection heat transfer from a thin horizontal isothermal plate in air-filled rectangular enclosure. J. Thermal Sci. Technol., 55–65 (2009)

[12] Meng, X. and Li, Y.: Numerical study of natural convection in a horizontal cylinder filled with water-based alumina nanofluid. Nanoscale Res. Lett. 10(42), 1–10 (2015)

[13] Xu, X., Yu, Z, Hu, Y, Fan, L, Cen, K: A numerical study of laminar natural convection heat transfer around a horizontal cylinder inside a concentric air filled triangular enclosure. Int. J. Heat Mass Transf. 53, 345–355 (2010)

[14] Seki, N., Fukusako, S. and Yamaguchi, A.: An experimental study of free convection heat transfer in a parallelogramic enclosure. ASME J. Heat Transf. 105, 433–439 (1983)

[15] ALdridy, K.D. and Yao, H.: Flow features of natural convection in a parallelogramic enclosure Int. Comm. Heat Mass Transf. 28, 923–931 (2001)

[16] Chung, K.C. and Trefethen, L.M.: Natural convection in a vertical stack of inclined parallelogrammic cavities. Int. J. Heat Mass Transf. 25(No.2), 277–284 (1982)

[17] Garcia de Maria, J.M., Bäiri, A. and Costa, V.A.F.: Empirical correlation at high Ra for steady-state free convection in 2D air-filled Parallelogrammic enclosures with discrete heat sources. Int. J. Heat Mass Transf. 53, 3831–3838 (2010)

[18] Bäiri, A., Zarco-Pernia, E., Garcia de Maria, J.M., Basin, J.G., Alilat, N., Laraqi, N., Gutierrez, F.: Nusselt-Rayleigh correlations for free convection in 2-D air filled parallelogrammic enclosures with isothermal active walls. Heat Mass Transf., 589–595 (2011)

[19] Costa, V.A.F.: Double-diffusive natural convection in parallelogram enclosures. Int. J. Heat Mass Transf. 47, 2913–2926 (2004)

[20] Costa, V.A.F., Oliveira, M.S.A., Sousa, A.C.M.: Laminar natural convection in a vertical stack of parallelogrammic partial enclosures with variable geometry. Int. J. Heat Mass Transf. 48, 779–792 (2005)

[21] Baïri, A.: On the Nusselt number definition adapted to natural convection in parallelogrammic cavities. Appl. Therm. Eng. 28, 1267–1271 (2008)

[22] Villeneuve, T., Boudreau, M., Dumas, G.: The thermal diode and insulating potentials of a vertical stack of parallelogrammic air filled enclosures. Int. J. Heat Mass Transf. 108 2060–2071 (2017)

[23] Costa, V.A.F.: Double-diffusive natural convection in PARALLELOGRAMMIC enclosure filled with fluid saturated porous media. Int. J. Heat Mass Transf. 47, 2699–2714 (2004)

[24] Hun Sik, H., Hyun, J.H.: Buoyant convection in a parallelogrammic enclosure filled with a porous medium—general analysis and numerical simulations. Int. J. Heat Mass Transf. 51 29980-2989 (2008)

[25] Jagadeesha, R.D., Prasanna, B.M.R., Sankar, M.: Numerical simulation of double diffusive magneto convection in an inclined parallelogrammic porous enclosure with an internal heat source. Mater. Today Proc. 4, 10544–10548 (2017)

[26] Anandalakshmi, R. and Basak, T.: Heat flow visualization analysis on natural convection in rhombic enclosures with isothermal hot side or bottom wall. Eur. J. Mech. B/Fluids 41, 29–45 (2013)

[27] Anandalakshmi, R. and Basak, T.: Natural convection in rhombic enclosures with isothermally heated side or bottom wall: entropy generation analysis. Eur. J. Mech. B/Fluids 54, 27–44 (2015)

[28] Baïri, A., Garcia de Maria, J.M., Laraqi, N.: Transient natural convection in parallelogrammic enclosures with isothermal hot wall. Experimental and numerical study applied to on-board electronics. Appl. Therm. Eng. 30, 1115–1125 (2010)

[29] Baïri, E.Z.P., Laraqi, N. and Garcia de Maria, J.M.: Transient free convection in parallelogrammic cavities applied to the thermoregulation of avionics. Int. J. Eng. Syst. Model. Simul. 2(Nos.1/2), 58-64 (2010)

[30] Baïri, A., Zacro Pernia, E., Garcia de Maria, J.M.: A review on natural convection in enclosures for engineering applications. The particular case of the parallelogrammic diode cavity. Appl. Therm. Eng. 63, 304–322 (2014)

[31] Hussain, S.H., Hussein, A.K. and Kadim, K.A.: Numerical simulation of natural convection in a paralellogrammic enclosure containing volumetric heat source with non-uniform heated left sidwall. Heat Transf. Asian Res. 43(6), 542–560 (2014)

[32] Jagadeesha, R.D., Prasanna, B.M.R, Sanger, M: Double diffusive convection in an inclined parallelogrammic porous enclosure. Int. Conf. Comput. Heat Mass Transf., 1346–1353 (2015)

[33] Jagadeesha, R.D., Prasanna, B.M.R., Younger, D. and Sanger, M.: Natural convection in an inclined parallelogrammic porous enclosure under the effect of magnetic field. J. Phys. Conf. Series 908, 1–9 (2017)

[34] Das, D., Roy, M. and Basak, T.: Studies on natural convection within enclosures of various (non-square) shapes—a review. Int. J. Heat Mass Transf. 106, 356–406 (2017)

[35] Basak, T., Chamkha, A.J.: Heatline analysis on natural convection for nanofluids confined within square cavities with various thermal boundary conditions Int. J. Heat Mass Transf. 55 5526–5543 (2012)

[36] Oztop, H.F., Mobedi, M., Abu-Nada, E., Pop, I.: A heatline analysis of natural convection in a square inclined enclosure filled with a CuO nanofluid under non-uniform wall heating condition. Int. Heat Mass Transf. 55, 5076–5086 (2012)

[37] Moradi, H., Bazooyar, B., Etemad, S.G., Moheb, A.: Influence of geometry of cylindrical enclosure on natural convection heat transfer of Newtonian fluids. Chem. Eng. Res. Des. 94, 673–680 (2015)

[38] Hussain, S.H., Hussein, A.K.: Natural convection heat transfer enhancement in a differentially heated parallelogrammic enclosure filled with copper-water nanofluid. J. Heat Transf. 136, 1–8 (2014)

[39] Ghalambaz, M., Mikhail, Z., Sheremet, A., Pop, I.: Free convection in a parallelogrammic porous cavity filled with a nanofluid using Tiwari and Das nanofluid model. PLOs One J., 1–17 (2015)

[40] Alsabery, A.I., Chamkha, A.J., Hussain, S.H., Saleh, H., Hashim, I.: Heatline visualization of natural convection in a trapezoidal cavity partly filled with nanofluid porous layer and partly with non-Newtonian fluid layer. Adv. Powder Technol. 26, 1230–1244 (2015)

[41] Selimefendigil, F., Oztop, H.F., Abu-Hamdeh, N.: Natural convection and entropy generation in nanofluid filled entrapped trapezoidal cavities under the influence of magnetic field. Entropy 18(43), 2–22 (2016)

[42] Alsabery, A.I., Chamkha, A.J., Sahe, H., Hashim, I.: Heatline visualization of conjugate natural convection in a square cavity filled with nanofluid with sinusoidal temperature variations on both horizontal walls. Int. J Heat Transf. 100, 835–850 (2016)

[43] Wang, X.F., Dai, W.: Heatline analysis on heat transfer and convective flow of nanofluid in an inclined enclosure. Heat Transf. Eng. 39(10), 843–860 (2018)

[44] Mehryan, S.A.M., Kaskooli, F.M., Ghalambaz, M., Chamkha, A.J: Free convection of hybrid Al_2O_3-Cu water nanofluid in a differentially heat porous cavity. Adv. Powder Technol. 28(9) 2295–2305 (2017)

[45] Syam Sundar, L., Sharma, K.V., Singh, M.K., C.M.S , A.: Hybrid nanofluid preparation, thermal properties, heat transfer and friction factor— a review. Renewable Sustainable Energy Rev. 68, 185–198 (2017)

[46] Fahad Sadekin Zaman, T. Saha Turja, M.D., Molla, M.: Buoyancy driven natural convection flow in an enclosure with two discrete heating from below. Proc. Eng. 56, 104–111 (2013)

[47] Zhang, T., Che, D.: Double MRT thermal Lattice Boltzman simulation for MHD natural convection of nanofluids in an inclined cavity with four square heat sources. Int. J. Heat Mass Transf. 94, 87–100 (2016)

[48] Bouraoui, A., Bessaïh, R.: Three-dimensional steady and oscillatory natural convection in a rectangular enclosure with heat sources. J. Heat Transf. 138, 1–8 (2016)

[49] Refai Ahmed, G., Yovanovich, M.M.: Influence of discrete heat source location on natural convection of heat transfer in a vertical square enclosure. Trans. ASME 113, 268–274 (1991)

[50] Chadwick, M.L., Webb, B.W., Heaton, H.S. Natural convection from two-dimensional discrete heat sources in a rectangular enclosure. Int. J. Heat Mass Transf. 34(No.7), 1679–1693 (1991)

[51] Keyhani, M., Chen, L., Pitts, D.R.: The aspect ratio effect on natural convection in an enclosure with protruding heat source. J. Heat Transf. 113, 883–891 (1991)

[52] Chadwick, M.L., Webb, B.W., Heaton, H.S.: Natural convection from discrete heat sources in a vertically vented rectangular enclosure. Exp. Heat Transf. 4, 199–216 (1991)

[53] Refai Ahmed, G., Yovanovich, M.M.: Numerical study of natural convection from discrete heat sources in vertical square enclosure. J. Themophysics 6(No.1), 121–127 (1992)

[54] Coates, M.J., Patterson, J.C.: Numerical Simulations of the natural convection in a cavity with non-uniform internal sources. Int. J. Heat Fluid Flow 15(No.3), 218–225 (1994)

[55] Al-Bahi, A., Al-Hazmy, M., Zaki, G.M.: Natural convection in a tilted rectangular enclosure with a single discrete heater. JKAU: Eng. Sci 16(No.2), 117–136 (2005)

[56] Aminossadati, S.M., Ghasemi, B.: Natural convection of a localized heat source at the bottom of a nanofluid-filled enclosure. Eur. J. Mech. B/Fluids 28, 630–640 (2009)

[57] Narasimham, G.S.V.L.: Natural convection from discrete heat sources in enclosure: an overview VIVECHAN. Int. J. Res. 1, 63–78 (2010)

[58] Baïri, A., Garcia de Maria, J.M., Baïri, I., Laraqi, N., Zacro-Pernia, E., Alilta, N.: 2D transient natural convection in diod cavities containing electronic equipment with discrete active bands under constant heat flux. Int. J. Heat Mass Transf. 55, 4970–4980 (2012)

[59] Sankar, M., Kim, B, Lopez, J.M.: Younghae Do Thermsolutal convection from a discrete heat and solute source in a vertical porous annulus. Int. J. Heat Mass Transf. (2012)

[60] Takabi, B. and Salehi, S.: Augmentation of the heat transfer performance of sinusoidal corrugated enclosure by employing hybrid nanofluid. Adv. Mech. Eng. (2014)

[61] Elsherbiny, S.M., Ismail, O.I.: Heat transfer in inclined air rectangular cavities with two localized heat sources. Alex. Eng. J. 54, 917–927 (2015)

[62] Cho, C-C., Yau, H-T., Chiu, C-H. and Chiu, K-C.: Numerical investigation into natural convection and entropy generation in a nanofluid-filled U-shaped cavity. Entropy 17, 5980–5994 (2015)

[63] Das, D., Basak, T.: Role of distributed/discrete solar heaters for the entropy generation studies in the square and triangular cavities during natural convection. Appl. Thermal Sci. 113, 1514–1535 (2017)

[64] Hussein, A.K., Hadi Hussain, S.: Heatline visualization of natural convection heat transfer in an inclined wavy cavities filld with nanofluid and subjected to a discrete isoflux heating from its left sidewall. Alex. Eng. J 55, 169–186 (2016)

[65] Nithyadevi, N., Divya, V. and Rajarathinan, M.: Effect of Prandtl number on natural convection in a rectangular enclosure with discrete heaters. J. Appl. Sci. Eng. 20(No.2), 173–182 (2017)

[66] Oztop, H.F., Abu-Nada, E.: Numerical study of natural convection in partially heated rectangular enclosures filled with nanofluids. Int. J. Heat Fluid Flow 29, 1326–1336 (2008)

[67] Bondareva, N.S, Sheremet, M.A, Oztop, H.F, Abu-Hamdeh, N: Entropy generation due to natural convection of a nanofluid in a partially open triangular cavity. Adv. Powder Technol. 28(1), 244–255 (2017)

[68] Shermet, M., Pop, I., Oztop, H.F., Abu-Hamdeh, N.: Natural convection of nanofluid inside a wavy cavity with a non-uniform heating: entropy generation analysis. Int. J. Numer. Methods Heat Fluid Flow 27(4), 1–31 (2017)

[69] Selimefengdigil, F., Oztop, H.F.: Mixed convection of nanofluids in a three dimensional cavity with two adiabatic inner rotating cylinder. Int. J. Heat Mass Transfer 117, 331–343 (2018)

[70] Brinkman, H.C.: The viscosity of concentrated suspensions and solution. J. Chem. Phys. 20, 571–581 (1952)

[71] Maxwell, J., A Treatise on Electricity and Magnetism, 2nd ed. Oxford University Press, Cambridge, UK (1904)

[72] Basak, T., Aravind, G., Roy, S., Balakrishnan, A.R.: Heatline analysis of heat recovery and thermal transport in materials confined within triangular cavities. Int. J. Heat Mass Transf. 53 3615–3628 (2010)

[73] Rannacher, R.: On Chorin's Projection Method for the Incompressible Navier-Stokes Equations, In "Navier-Stokes Equations: Theory and Numerical Methods, (R. Rautmann, et al., eds.), Proc. Oberwolfach Conf., 19–23 (1991)